FU JEN STUDIES

NATURAL SCIENCES

NO. 16 1982

CONTENTS

FU JEN UNIVERSITY

TAIPEI, TAIWAN, REPUBLIC OF CHINA

THE EXCHANGE ANISOTROPY OF MnF_2 AT 0°K IN NEARLY CUBIC SYMMETRY APPROXIMATION

KOW-JE LING, MING-CHANG HUANG
and NAI-LI HUANG-LIU

ABSTRACT

Recently Barak *et al.* have experimentally obtained the exchange anisotropy of MnF_2. In this paper a calculation of exchange anisotropy for MnF_2, considering the electronic configuration in detail with nearly cubic symmetry approximation, is presented. The result obtained is numerically acceptable in comparison with the experimental result obtained by Barak *et al.*

I. INTRODUCTION

MnF_2 is a typical antiferromagnet with Neel temperature at 66.5°K. The magnetic and chemical unit cells are of the same size. The Mn^{2+} ions form an easy axis, two sublattice, uniaxial antiferromagnet, with the spins on the corner oppositely directed to the spin in the body-center. The crystal parameters were determined by X-ray diffraction as $c=3.3003$ Å and $a=4.8732$ Å.[1] The major contribution to the anisotropic energy comes from the magnetic dipole interaction and single ion anisotropy, at temperature both above[2] and below[3] T_c, where the contribution due to exchange interaction is very small. Recently Barak *et al.*[4] have determined experimentally the exchange anisotropy. In this paper a treatment of exchange interaction, considering the electronic configuration in detail with nearly cubic symmetry approximation, is presented. In MnF_2 a strong exchange interaction exists between the center and the corner spins which are directed oppositely. In addition there is a weaker exchange interaction between two nearest corner spins or the center spins, directed parallelly. This weaker interaction is neglected in this paper.[3] In section II, first the form of the exchange Hamiltonian and the method of calculating it are discussed,

and then we find the ionic ground state wave functions of Mn^{2+} in nearly cubic crystalline field, considering the spin-orbit coupling as perturbation to first order. Besides these the covalency effect due to F^- ions is also neglected. We use this result to calculate the exchange anisotropy. Finally this result is compared with the experimental value obtained by Barak *et al.*

II. THE CALCULATION OF THE ANISOTROPIC EXCHANGE BETWEEN Mn^{2+} IONS IN A NEARLY CUBIC SYMMETRY APPROXIMATION

If the orthogonal wave functions without considering the spin-orbit coupling are chosen as basis, the exchange interaction between the electrons of two ions can be written as

$$\mathcal{H}_{ex}^{ab} = -\sum_{i,j} j_{i,j} \vec{s}_i \cdot \vec{s}_j \qquad (1)$$

where i and j refer to the electrons belonging to ion a and b, respectively. If the wave function with the admixture of higher excited states due to spin-orbit coupling, are chosen as basis, and the ground states of the ions are orbitally non-degenerate, the above exchange Hamiltonian can be written as[5]

$$\mathcal{H}_{ex}^{ab} = -2J \vec{S}_a \cdot \vec{S}_b + \vec{D} \cdot (\vec{S}_a \times \vec{S}_b) + \vec{S}_a \cdot \overleftrightarrow{A} \cdot \vec{S}_b \qquad (2)$$

where the first term represents the isotropic exchange, the second term the antisymmetric exchange, and the last term the anisotropic exchange. In MnF_2 the second term vanishes because of the symmetry.[5] Further by considering the total exchange interaction between the center spin and the eight corner spins and the tetragonal symmetry of Mn^{+2} ion in MnF_2, one can reduce $\overleftrightarrow{A}$ to

$$\overleftrightarrow{A} = \begin{bmatrix} A_\perp & 0 & 0 \\ 0 & A_\perp & 0 \\ 0 & 0 & A_z \end{bmatrix}$$

Hence eq. (2) can be written as

$$\mathcal{H}_{ex}^{ab} = -[J_{ab}\vec{S}_a \cdot \vec{S}_b + J_A^z S_b^z S_a^z] \qquad (3)$$

where $J_{ab}=2J-A_\perp \approx 2J$ is the isotropic exchange, and $J_A^z = A_\perp - A_z$ is the anisotropic exchange.

To calculate J_{ab} and J_A^z, we shall equate the matrix elements of the effective exchange Hamiltonian evaluated within S=5/2 manifold for each ion to the corresponding matrix elements of the exchange Hamiltonian in eq. (1) evaluated by using the perturbed ^6S states with the consideration of anti-symmetry. This is done in the following.

The ground level of Mn^{2+} ion in a cubic crystalline field has been discussed by Watanabe,[6] Blume and Orbach,[7] and Sharma, Das and Orbach.[8] In the presence of a crystalline field, if the spin-orbit coupling is not considered, the ground state is ^6S. If the spin-orbit coupling is considered, only the excited $^4\Gamma_4$ states can be admixed into the ground state via spin-orbit coupling. The excited quartets which contain Γ_4 character are the ^4P, ^4F, and ^4G. The cubic crystalline field also admixes these three quartets into one another. We need to diagonalize the $^4\Gamma_4$ matrix in the presence of a cubic field to find the eigenfunctions of a cubic field. These three eigenfunctions which transform as $^4\Gamma_4$ are

$$|i\,^4\Gamma_4, j\rangle = \alpha_i |P\,^4\Gamma_4, j\rangle + \beta_i |F\,^4\Gamma_4, j\rangle + \gamma_i |G\,^4\Gamma_4, j\rangle \qquad (4)$$

where the subscript i distinguishes the three different $^4\Gamma_4$ states, and $j=\pm 1, 0$ denotes the three orbitally degenerates for a given $^4\Gamma_4$ state. The coefficients α_i, β_i, and γ_i are determined from the secular determinant of the cubic crystalline field.[8] The ground state of Mn^{2+} as perturbed by the spin-orbit coupling to the first order in cubic crystalline field is given by

$$|^6S, M_s\rangle_{\text{admixed}} = |^6S, M_s\rangle - \sum_{i,j,M_s'} \frac{\langle i\,^4\Gamma_4 j M_s' | \xi \sum_\mu \vec{l}_\mu \cdot \vec{S}_\mu | ^6S, M_s\rangle}{\Delta_i} \times |i\,^4\Gamma_4 j M_s'\rangle$$

where Δ_i is the energy difference between the ground state ^6S and

the excited state $i\,^4\Gamma_4$, and ξ is the spin-orbit constant, and μ refers to the electrons in the Mn^{2+} ion.

Since in MnF_2 the tetragonal distortion is much smaller than the cubic field, the perturbed ground state wave functions appropriate to a tetragonal crystalline field of nearly cubic symmetry can be approximately written as

$$
\begin{aligned}
&|{}^6S,\ M_s\rangle_{\text{admixed}} \\
&\quad = |\,{}^6S,\ M_s\rangle \\
&\qquad - \sum_{i,M_s'} \left\{ \frac{\langle i\,{}^4\Gamma_4\, 0M_s' \mid \xi \textstyle\sum_\mu \vec{l}_\mu \cdot \vec{S}_\mu \mid {}^6S,\ M_s\rangle}{\Delta_i''} \mid i\,{}^4\Gamma_4\, 0M_s'\rangle \right. \\
&\qquad \left. + \frac{\langle i\,{}^4\Gamma_4 \pm 1M_s' \mid \xi \textstyle\sum_\mu \vec{l}_\mu \cdot \vec{S}_\mu \mid {}^6S,\ M_s\rangle}{\Delta_i^{\perp}} \mid i\,{}^4\Gamma_4 \pm 1M_s'\rangle \right\} \qquad (5)
\end{aligned}
$$

where

$$\Delta_i'' = E({}^6S,\ M_s) - E(i\,{}^4\Gamma_4\, 0M_s)$$

$$\Delta_i^{\perp} = E({}^5S,\ M_s) - E(i\,{}^4\Gamma_4 \pm 1M_s)$$

The difference $\Delta_i'' - \Delta_i^{\perp}$ is roughly 250 cm^{-1}.[9] Using the above wave functions, we calculate the matrix elements of the Hamiltonian in eq. (3) between various states in $S^a = 5/2$ and $S^b = 5/2$ manifolds. We then equate these matrix elements to the corresponding ones obtained by evaluating the exchange Hamiltonian in eq. (1) between the perturbed ^6S states, i.e.,

$$
\begin{aligned}
&\langle (S^a = 5/2,\ M_s)\ (S^b = 5/2,\ M_s') \mid J_{ab}\, \vec{S}_a \cdot \vec{S}_b + J_A^z\, S_a^z\, S_b^z \mid \\
&\qquad (S^a = 5/2,\ M_s'')\ (S^b = 5/2,\ M_s''')\rangle \\
&\quad = \left\langle \psi^a_{M_s},\ \psi^b_{M_s'} \left| \sum_{i,j=1}^{5} j_{ij}\, \vec{s}_i \cdot \vec{s}_j \right| \psi^a_{M_s''},\ \psi^b_{M_s'''} \right\rangle \qquad (6)
\end{aligned}
$$

where $\psi^a_{M_s} \equiv |{}^6S,\ M_s\rangle_{\text{admixed}}$ as defined by eq. (5), is the antisymmetry wave function of five electrons in a Mn^{2+} ion; and $|(S^a = 5/2,\ M_s)\rangle$ represents the M_s component of $S^a = 5/2$ manifold. Doing this, we obtain the values of J_A^z and $J_\perp$ for the different substates M_s. Here we assume that j_{ij}'s are all equal, i.e. $j_{ij} = j_{avg}$.

for all i and j. These results are listed in Tables 1-3. As a check of our accuracy, we estimate $\Delta g/g$ by using our J_A^z / J_i. According to Orbach,[4] one would expect the ratio of J_A^z to J_i to be of the order of

$$\frac{J_A^z}{J_i} \approx \frac{1}{(2S)^2}\left(\frac{\Delta g}{g}\right)^2$$

where $\Delta g = g_{\parallel} - g_{\perp}$ is the anisotropy in g value, and $S=5/2$. The value of $\Delta g/g$ we obtained are acceptable in comparing with the experimental values obtained by Barak *et al.*[4]

Table 1. Different results obtained for $10\,Dq = 9{,}000\ cm^{-1}$

Case	$M_s=M_s'=M_s''=M_s'''$ chosen to find J_z'	$M_s=M_s'''=M_s^{(a)}$, $M_s'=M_s''=M_s^{(b)}$, chosen to find $J_\perp'$	$\frac{J_A}{J_i}$	$\frac{\Delta g}{g}$	$\Delta g^{(4)}$ (exp.)
1[15]	$\frac{5}{2}$	$M_s^{(a)}=\frac{5}{2}$, $M_s^{(b)}=\frac{3}{2}$	6.3×10^{-6}	1.3×10^{-2}	
2	$\frac{3}{2}$	$M_s^{(a)}=\frac{3}{2}$, $M_s^{(b)}=\frac{1}{2}$	3.9×10^{-6}	1.0×10^{-2}	
3	$\frac{1}{2}$	$M_s^{(a)}=\frac{1}{2}$, $M_s^{(b)}=-\frac{1}{2}$	1.6×10^{-5}	4.0×10^{-2}	$\ll10^{-2}$
4	$-\frac{1}{2}$	$M_s^{(a)}=-\frac{1}{2}$, $M_s^{(b)}=-\frac{3}{2}$	1.2×10^{-5}	3.0×10^{-2}	
5	$-\frac{3}{2}$	$M_s^{(a)}=-\frac{3}{2}$, $M_s^{(b)}=-\frac{5}{2}$	1.6×10^{-5}	4.0×10^{-2}	

III. DISCUSSION

In this paper we have derived the contributions, of the mixing

of the excited configuration of the Mn^{2+} ion into the ground configuration via the spin-orbit coupling, to the exchange anisotropy in MnF_2. We found that these contributions are numerically acceptable in comparison with the experimental result. But we have neglected the following effects in our treatment:

a) Since the major contribution to the exchange interaction between the center and the corner spins is due to super-exchange,[10] the covalent mixing of F^- states into Mn^{2+} states should be taken into account. Barak *et al.* have concluded qualitatively that this effect could reduce the theoretical estimation.

b) The 4D excited state, which is not admixed into the ground state via the spin-orbit coupling in the cubic crystalline field, will be admixed in the tetragonal crystalline field. In our treatment, the effect has also been neglected. This may explain why our values

Table 2. Different results obtained for $10\,Dq = 10{,}000\ cm^{-1}$

Case	$M_s = M_s' = M_s'' = M_s'''$ chosen to find J_z'	$M_s = M_s''' = M_s^{(a)}$, $M_s' = M_s'' = M_s^{(b)}$, chosen to find $J_\perp'$	$\frac{J_A}{J_i}$	$\frac{\Delta g}{g}$	$\Delta g^{(4)}$ (exp.)
1[15]	$\frac{5}{2}$	$M_s^{(a)} = \frac{5}{2}$, $M_s^{(b)} = \frac{3}{2}$	6.8×10^{-6}	1.3×10^{-2}	
2	$\frac{3}{2}$	$M_s^{(a)} = \frac{3}{2}$, $M_s^{(b)} = \frac{1}{2}$	4.5×10^{-6}	1.1×10^{-2}	
3	$\frac{1}{2}$	$M_s^{(a)} = \frac{1}{2}$, $M_s^{(b)} = -\frac{1}{2}$	1.8×10^{-5}	4.4×10^{-2}	$\ll10^{-2}$
4	$-\frac{1}{2}$	$M_s^{(a)} = -\frac{1}{2}$, $M_s^{(b)} = -\frac{3}{2}$	1.4×10^{-5}	3.3×10^{-2}	
5	$-\frac{3}{2}$	$M_s^{(a)} = -\frac{3}{2}$, $M_s^{(b)} = -\frac{5}{2}$	1.8×10^{-5}	4.4×10^{-2}	

Table 3. Different results obtained for $10\,Dq = 11{,}000\ cm^{-1}$

Case	$M_s = M_s' = M_s'' = M_s'''$ chosen to find J_z'	$M_s = M_s''' = M_s^{(a)}$, $M_s' = M_s'' = M_s^{(b)}$, chosen to find $J_\perp'$	$\frac{J_A}{J_i}$	$\frac{\Delta g}{g}$	$\Delta g^{(4)}$ (exp.)
1[11]	$\frac{5}{2}$	$M_s^{(a)} = \frac{5}{2}$, $M_s^{(b)} = \frac{3}{2}$	7.8×10^{-6}	1.4×10^{-2}	
2	$\frac{3}{2}$	$M_s^{(a)} = \frac{3}{2}$, $M_s^{(b)} = \frac{1}{2}$	5.2×10^{-6}	1.2×10^{-2}	
3	$\frac{1}{2}$	$M_s^{(a)} = \frac{1}{2}$, $M_s^{(b)} = -\frac{1}{2}$	2.1×10^{-5}	4.8×10^{-2}	$\ll10^{-2}$
4	$-\frac{1}{2}$	$M_s^{(a)} = -\frac{1}{2}$, $M_s^{(b)} = -\frac{3}{2}$	1.6×10^{-5}	3.6×10^{-2}	
5	$-\frac{3}{2}$	$M_s^{(a)} = -\frac{3}{2}$, $M_s^{(b)} = -\frac{5}{2}$	2.1×10^{-5}	4.8×10^{-2}	

for J' and J_z' depend on M_s. In a more refined calculation, one should consider the mixing of ^4D into the ^6S state of Mn^{2+} ion. This work is currently being carried out.

REFERENCES

(1) D. F. Gibbsons, *Phys. Rev.* **115**, 1194 (1959).
(2) F. Keffer, *Phys. Rev.* **87**, 608 (1952).
(3) T. Oquchi, *Phys. Rev.* **111**, 1063 1958).
(4) J. Barak, V. Jaccarina and S. M. Rezende, *J. Magn. Matter.* 9(4), 323 (1978).
(5) T. Moriya, *Phys. Rev.* **120**, 91 (1960).
(6) H. Watanabe, *Proc. Theor. Phys.* **18**, 495 (1957).
(7) M. Blume and R. Orbach, *Phys. Rev.* **127**, 1587 (1962).
(8) R. R. Sharma, T. P. Das, and R. Orbach, *Phys. Rev.* **149**, 257 (1966).
(9) B. N. Figgis, "*Introduction to Ligand Fields*" (John Wiley & Sons 1966).

(10) P. W. Anderson, *Phys. Rev.* **115**, 2 (1959).
(11) This result is obtained by treating spin-orbit coupling as perturbation up to second order.

ION-MOLECULE DIFFERENTIAL CROSS SECTIONS AND ENERGY TRANSFER DISTRIBUTIONS

FRANK E. BUDENHOLZER SVD and CHING-CHING LEE

I. INTRODUCTION

We have previously reported methods to calculate non-reactive total (that is summed over all final states) differential cross sections and rotational energy transfer distributions at fixed scattering angles for low energy atomic ion-linear molecule collisions.[1] We here apply these methods to the Li^+-CO and Li^+-N_2 systems and compare the results with experiment.

II. DIFFERENTIAL CROSS SECTIONS

The potential between an atomic ion and a small linear molecule can be expressed as a sum over Legendre polynomials,

$$V(R, \psi) = \sum_{l=0}^{n} V_l(R) P_l(\cos\psi) \tag{1}$$

where R is the distance between the ion and the linear molecule center of mass, ψ the angle between R and the molecular axis, $V_l(R)$ potential terms generally in inverse powers of R, and P_l the Legendre polynomials.

We define the reduced scattering angle $\tau = E\vartheta$ where E is the center of mass energy of the collision and ϑ is the polar deflection angle. For a potential of the form of eq. (1) classical perturbation scattering theory (CPST) may be used to determine τ as a closed function of the impact parameter b and angles α and β defining the initial orientation of the molecule in a space fixed coordinate system.[2]

$$\tau = \tau(b, \alpha, \beta). \tag{2}$$

Using Monte Carlo techniques we then calculate a reduced differential cross section $\rho(\tau)$

$$\rho(\tau) = \vartheta I(\vartheta) \sin \vartheta \qquad (3)$$

where $I(\vartheta)$ is the differential cross section.[8]

In Figs. 1 to 4 we display the results for the Li^+-CO and Li^+-N_2 systems. In these calculations the spherically symmetric V_0 potential is a special function related to the MSV potential. It

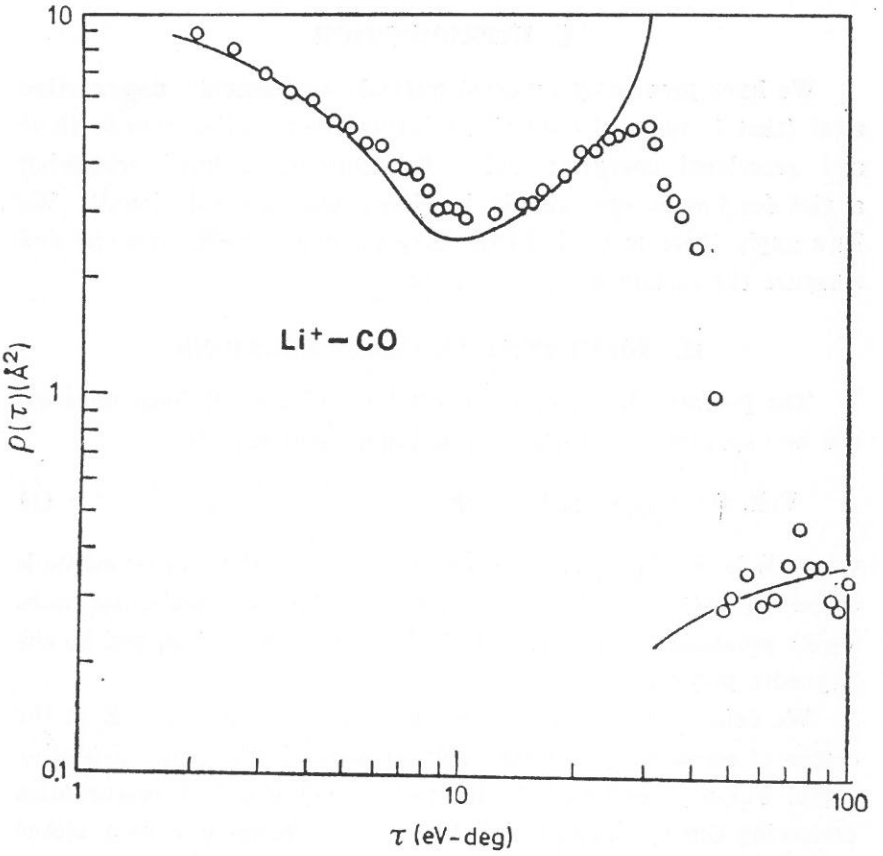

Fig. 1. The reduced differential cross section $\rho(\tau)$ plotted against the reduced deflection angle τ for the Li^+-CO system. The anisotropic part of the potential includes a quadrupole term with quadrupole moment 2.0×10^{-6}esu cm² and a dipole term with dipole 0.112 Debye. The symmetric part of the potentialis is from the experimental work of Polak-Dingels.[7] The circles are calculated using the complete potential; the solid line is the cross section obtained when only the spherically symmetric part of the potential is used. 2.0×10^5 trajectories were run.

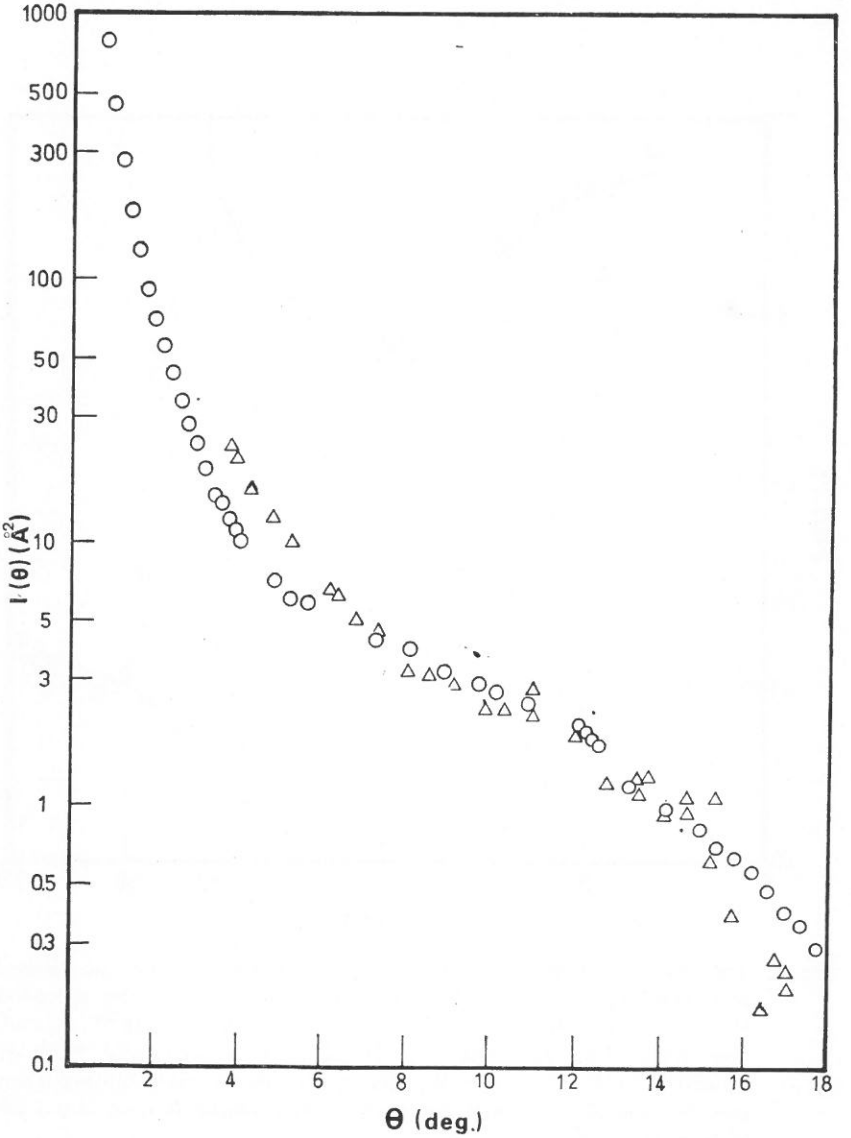

Fig. 2. The differential cross section $I(\vartheta)$ plotted against the deflection angle ϑ for Li^+-CO. The cross section is the same as that of Fig. 1, calculated for a collision energy of E = 2.47 eV. The circles are our results, the triangles the experimental results of ref. 8.

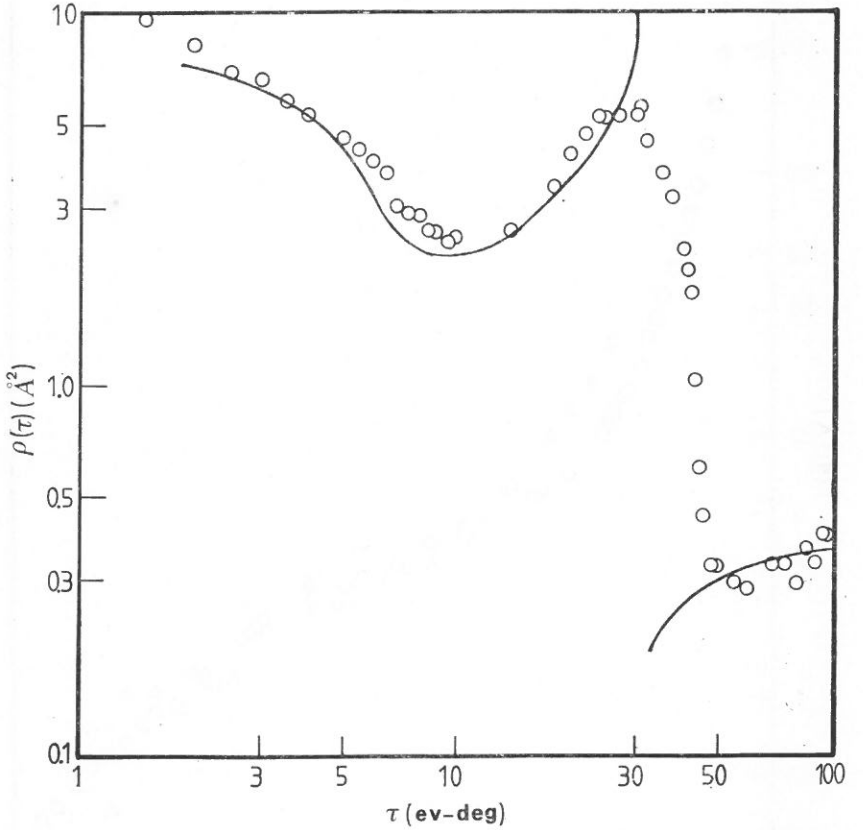

Fig. 3. The reduced differential cross section $\rho(\tau)$ plotted against the reduced deflection angle τ for Li^+-N_2. The anisotropic part of the potential is a quadrupole term with quadrupole moment 1.5×10^{-26} esu cm^2. The spherically symmetric part is from the experimental work of Polak-Dingels.[7] The solid line shows the cross section obtained when only the spherically symmetric part of the potential is used. 2.0×10^5 trajectories were run.

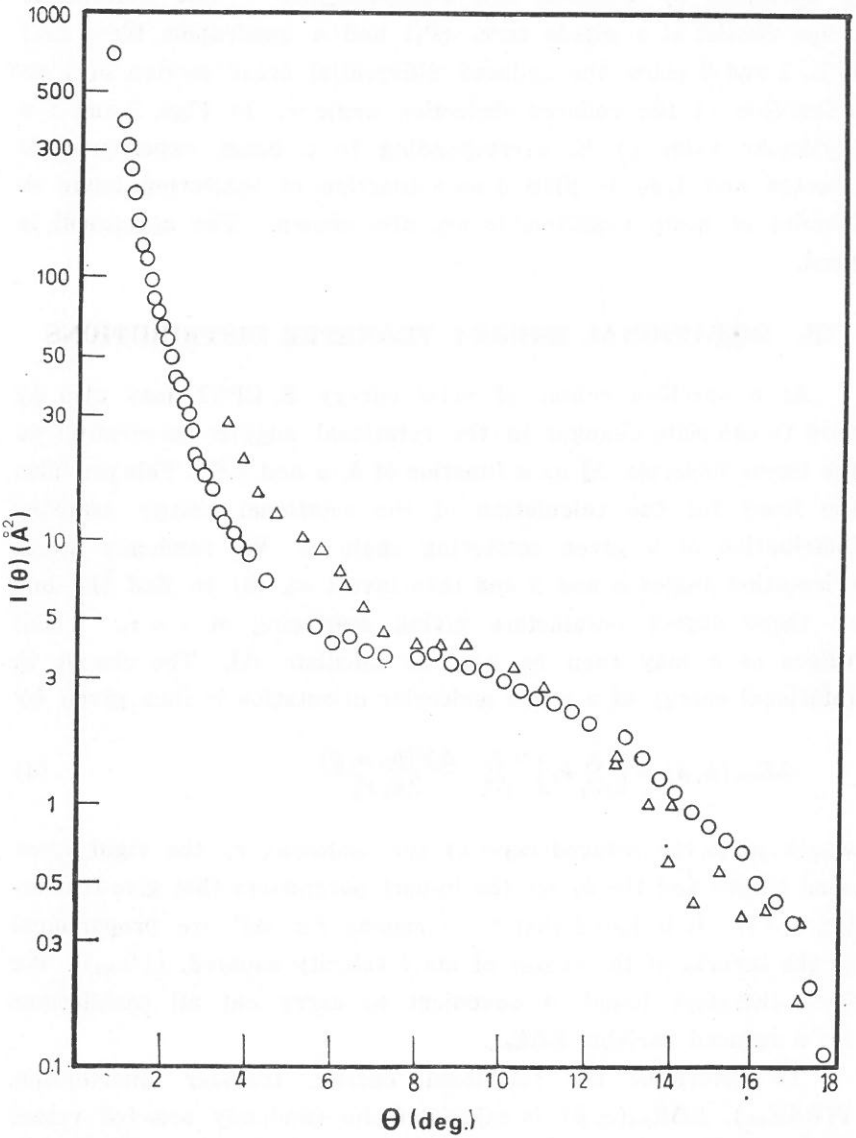

Fig. 4. The differential cross section $I(\vartheta)$ versus deflection angle ϑ for Li^+-N_2. The cross section is the same as that of Fig. 3, calculated for a collision energy of 2.47 eV. Circles are our results, the triangles experimental results from ref. 8.

is described by Gislason and Polak-Dingels.[4] The anisotropic terms consist of a dipole term (P_1) and a quadrupole term (P_2) Figs. 1 and 3 show the reduced differential cross section $\rho(\tau)$ as a function of the reduced deflection angle τ. In Figs. 2 and 4 a particular value of E, corresponding to a beam experiment, is selected and $I(\vartheta)$ is plotted as a function of scattering angle ϑ. Results of beam experiments are also shown. The agreement is good.

III. ROTATIONAL ENERGY TRANSFER DISTRIBUTIONS

At a specified center of mass energy E, CPST may also be used to calculate changes in the rotational angular momentum of the linear molecule ΔJ as a function of b, α and β.[5] This provides the basis for the calculation of the rotational energy transfer distribution at a given scattering angle τ_0. We randomly select orientation angles α and β and then invert eq. (2) to find the one or three impact parameters giving scattering at $\tau = \tau_0$. These values of b may then be used to calculate ΔJ. The change in rotational energy at a given molecular orientation is then given by

$$\Delta E_{rot}(\alpha, \beta) = \left[\sum_{i=1}^{3} b_i\right]^{-1} \sum_{i=1}^{3} \frac{\Delta J^2(b_i, \alpha, \beta)}{2\mu_D r_e^2} \tag{4}$$

where μ_D is the reduced mass of the molecule, r_e the rigid rotor bond length and the b_i are the impact parameters that give scattering $\tau = \tau_0$. It is found that the formulas for ΔJ^2 are proportional to the inverse of the center of mass velocity squared, $(1/v_{cm})^2$. We have therefore found it covenient to carry out all caclulations for a reduced variable $E\Delta E_{rot}$.

To determine the rotational energy transfer distribution, $P(E\Delta E_{rot})$, $E\Delta E_{rot}(\alpha, \beta)$ is calculated for randomly selected values of α and β. If these values are "binned" the usual histogram distribution is obtained. We have chosen to expand the distributions in a Fourier series in a way analogous to that described by Kosmos and coworkers.[6].

Figures 5 and 6 show the distributions obtained for various values

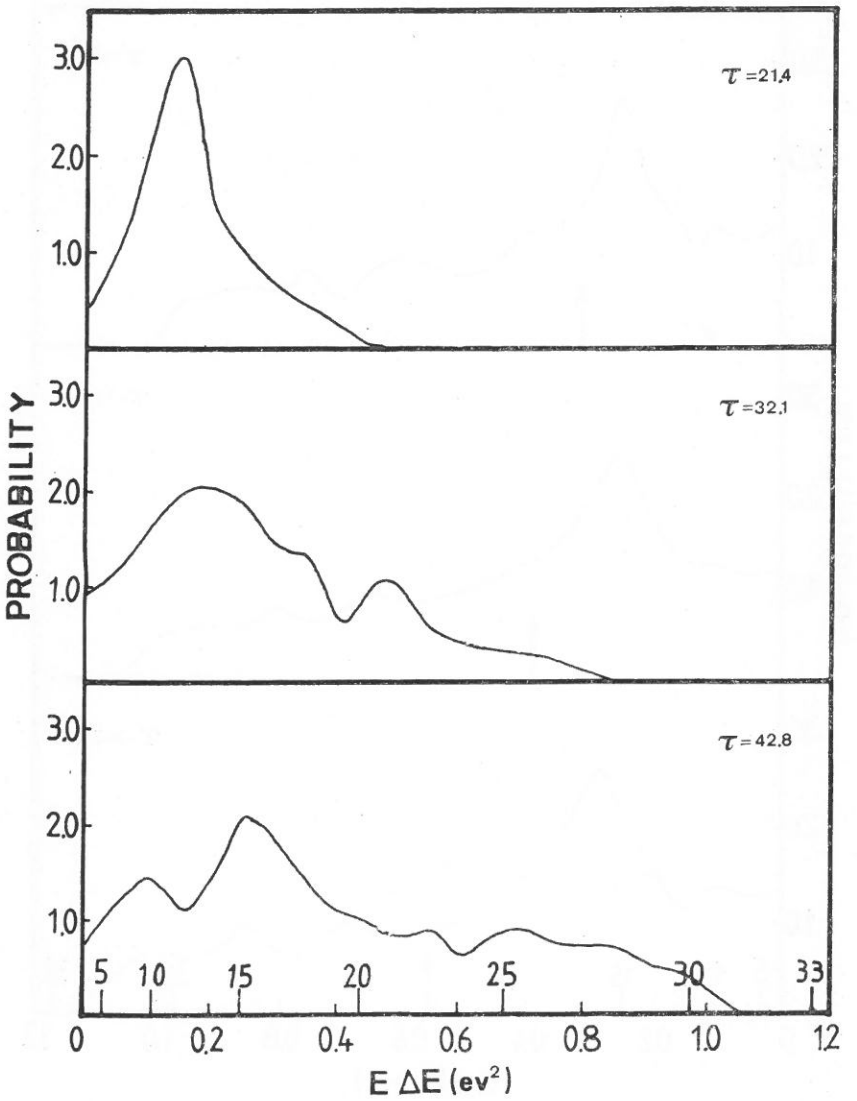

Fig. 5. Rotational energy transfer distributions at the reduced scattering angles τ for Li^+-CO. The calculations were done using the potential parameters discussed under Fig. 1. The lower abscissa scale is in the units of the calculation, eV^2. The upper scale shows the final rotational quantum number (presuming initial $J = 0$) for $E = 4.28$ eV. These figures may be compared with the time of flight spectra of ref. 9.

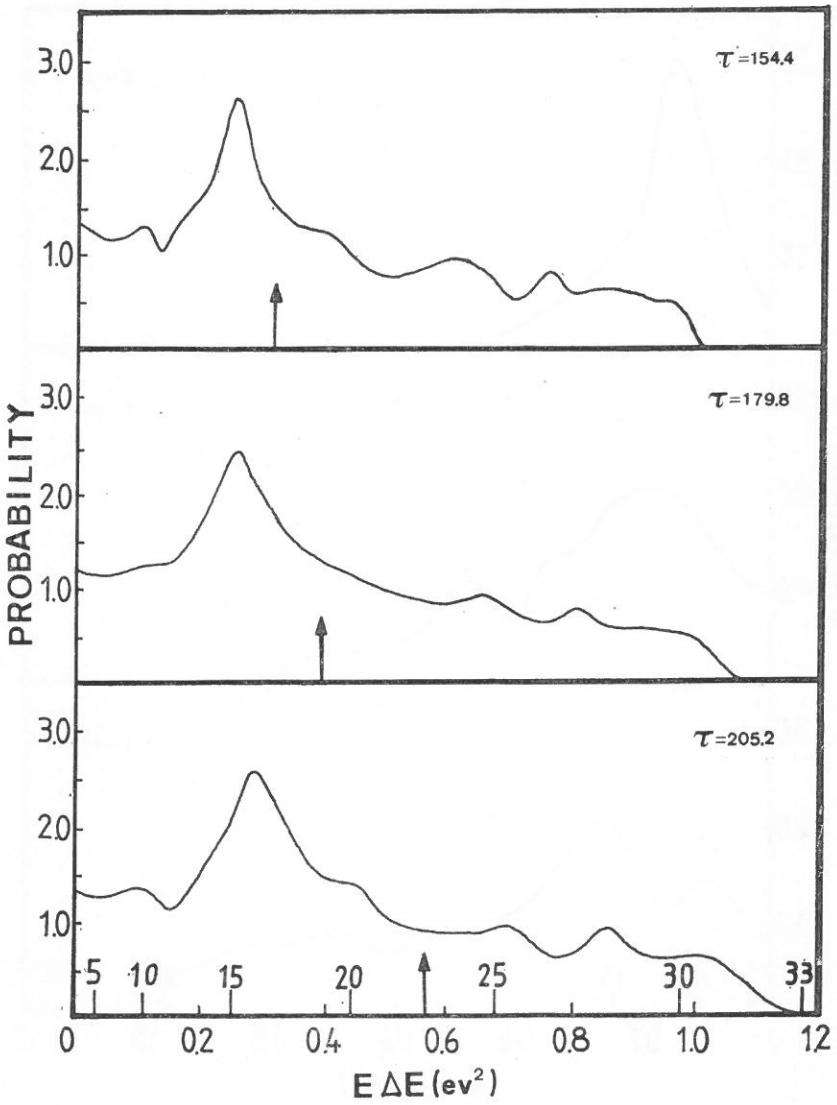

Fig. 6. Potential energy transfer distributions at the indicated reduced scattering angles τ for Li^+–N_2. The calculations were done using the potential parameters described under Fig. 3. The lower abscissa scale is in the units of the calculation eV^2. The upper scale shows the final rotational quantum numbers for E = 4.23 eV. The arrows indicate the maxima in experimental distributions given in ref. 10. The poor agreement with experiment for the $\tau = 205.2$ eV deg. distribution is surely due in part to the breakdown of the CPST approximations for the relatively large scattering angle (42.5 deg.) at which the experiment was carried out.

of τ for the Li^+-CO and Li^+-N_2 systems. Note that two abscissa scales are shown. The lower is $E\Delta E$ in eV^2. The upper is the final rotational quantum number J_f, where we presume that the rotor is originally in the $J=0$ state and that the collision takes place at the indicated energy. Arrows in the Li^+-N_2 distributions indicate the maxima of the experimental distributions.

IV. DISCUSSION

Both the differential cross section and the energy transfer distributions may be formally defined in terms of the delta function:

$$\frac{\rho(\tau_0)}{\tau_0} = \frac{1}{4\pi}\int_0^{\pi}\sin\beta\, d\beta\int_0^{2\pi} d\alpha\int_0^{\infty} b db\,\delta[\tau(\alpha,\beta,b)-\tau_0] \tag{5}$$

$$P(\Delta E^0) = \frac{1}{4\pi}\int_0^{\pi}\sin\beta\, d\beta\int_0^{2\pi} d\alpha\,\delta[\Delta E(\alpha,\beta)-\Delta E^0]. \tag{6}$$

If the $\tau(\alpha,\beta,b)$ or $\Delta E(\alpha,\beta)$ "surfaces" have maxima, minima or saddle points, then singularities will appear: the classical rainbow in the case of eq. 5 (see Figs. 1 and 3) and the rotational rainbow in the case of eq. 6. In complex systems these rainbow singularities are normally quenched. However remnants of the rainbows can clearly be seen in both the differential cross sections and the energy transfer distributions.

V. ACKNOWLEDGEMENT

Acknowledgement is made to the National Science Council of the Republic of China for support of this work. Students King-He Lee and Ing-Lang Wu and assistant Ming-Hsiung Chang assisted with computer programming.

REFERENCES

(1) F. E. Budenholzer and C. C. Lee, *Chem. Phys.* 73 (1982) 323.
(2) E. A. Gislason and J. G. Sachs, *Chem. Phys.* 25 (1977) 155.
(3) F. E. Budenholzer and E. A. Gislason, *J. Chem. Phys.* 69 (1979) 4222.
(4) P. Polak-Dingels, M. S. Rajan and E. A. Gislason, *J. Chem. Phys.* 77 (1982) 3983.

(5) J. G. Sachs, *Ph. D. Thesis*, University of Illinois at Chicago (1978).
(6) A. Kosmos, E. A. Gislason and A. D. Jorgensen, *J. Chem. Phys.* **75** (1981) 2884.
(7) P. M. Polak-Dingels, *Ph. D. Thesis*, University of Illinois at Chicago (1979).
(8) U. Böttner, U. Ross, and J. P. Toennies, *J. Chem. Phys.* **65** (1976) 733.
(9) W. Eastes, U. Ross, and J. P. Toennies, *Chem. Phys.* **39** (1979) 407.
(10) D. Poppe and R. Böttner, *Chem. Phys.* **30** (1978) 375.

STUDIES ON THE CATIONIC PHOTOPOLYMERIZATION OF EPOXY RESINS

DONG-TSAIR HWANG, JONQ-MIN LIU
and SUNG-NUNG LEE

1. INTRODUCTION

Thermally-hardened epoxy resins of various types are well known to have an excellent range of properties:[1] electrical characteristics, chemical resistance, heat stability, adhesion to substrates, mechanical properties, and so on. In view of the trend toward better properties in the coatings, it is not surprising that in electronics. and other industries, the development of photocrosslinkable systems able to give similar excellent properties is being taken as a very worth-while present-day target. One approach has been to develop photoinitiators for the cationic polymerization of epoxy compounds. There are three general classes that are currently of importance: aryldiazonium salts, diaryliodonium salts, and triarylsulfonium salts. All of these "onium" salts have a counter anion with low nucleophilicity, such as tetrafluoroborates or hexafluorophosphates. Although aryldiazonium salts were known to be cationic photoinitiators in the 1950's, the poor thermal stability and the gas evolving problem limit the use of diazonium salts in coatings and other applications.[2] The diaryliodonium and triarylsulfonium salts which have been developed and studied in more recent years as photoinitiators for epoxy polymerization do not suffer from these limitations, and consequently they have awakened quite considerable interest.[3-8]

Typical commercial epoxy resins (diglycidyl ether of bisphenol A, DGEBA) usually exhibit a glass transition temperature (Tg) in the range of 140°–170°C. Demands for even higher performance systems resulted from the electronic fields and aerospace fields. They continue to challenge the polymer chemist. By employing 9, 9′-bis

(4-hydroxyphenyl) fluorene instead of bisphenol A, an epoxy resin (diglycidyl ether of bisphenol fluorene, DGEBF) with better thermal property was synthesized.[9]

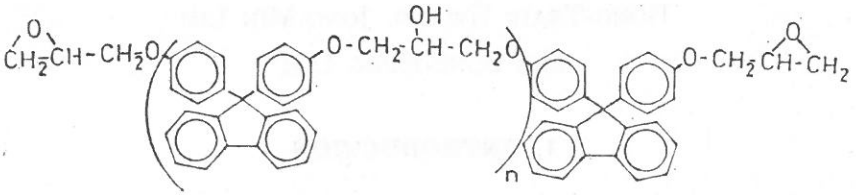

DGEBF $n=0, 1, 2, \cdots$

In this article, we report the use of diaryliodonium hexafluorophosphate as photoinitiator to study curing rates, and heat properties of epoxy resins including DGEBA, DGEBF, vinylcyclohexene dioxide (ERL-4206), and 3, 4-epoxy-6-methylcyclohexyl-3, 4-epoxy-6-methylcyclo-hexane carboxylate (ERL-4221).

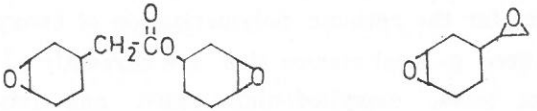

ERL-4221 ERL-4206

2. RESULTS AND DISCUSSIONS

The effects of initiator concentration on the curing rates and Tg's of cured ERL-4221 resin are shown in Fig. 1 and Fig. 2. Both curing rates and Tg's are increased with the initiator content. Theoretically, the cationic polymerization is a "living" process.[10] If this is true, the average molecular weight should be increased with the decrease of initiator content. However, the experimental results are inverse, the DSC study of the post cure of UV irradiated films gives exothermic curves. The exothermicity decreases with the increase of initiator content (Fig. 3). Apparently, terminating reactions caused by moisture absorbed are not negligibe. With more initiator content, the curing rate is faster the degree of polymerization is higher, and the Tg of the cured film results higher.

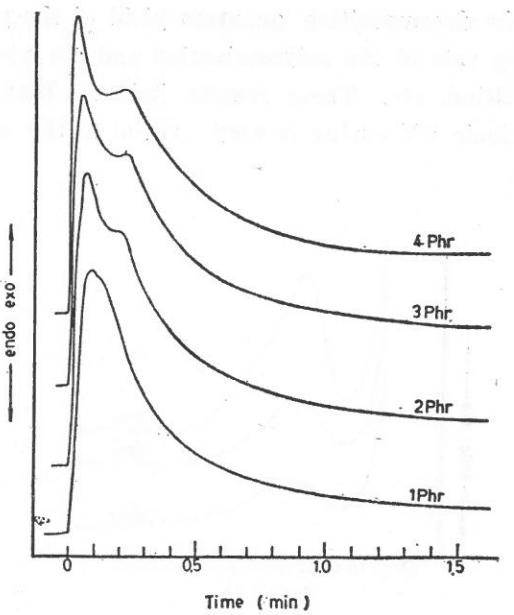

Fig. 1. Effect of initiator content on curing rate.

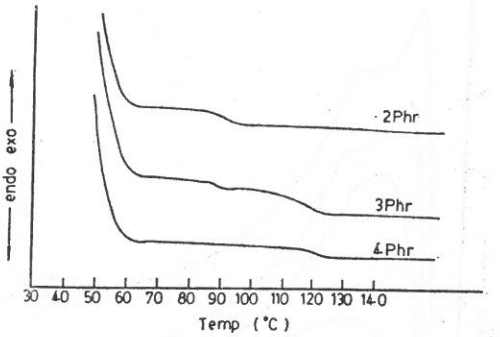

Fig. 2. Effect of initiator content on Tg's.

The effect of temperature on the curing rates and Tg's of ERL-4221 are shown in Fig. 4 and Fig. 5. Both curing rate and Tg increase with the curing temperature. The increasing of Tg's with temperature is a result of the higher degree of polymerization as shown in Fig. 6. The origin of the temperature influence on the curing rates may be very complicated. The possible parameters

involved are the decomposition quantum yield of the photoinitiator, the propagating rate of the polymerization and the viscosity of the curing composition, etc. These results indicate that temperature control of cationic UV curing is very crucial to the end-properties of cured films.

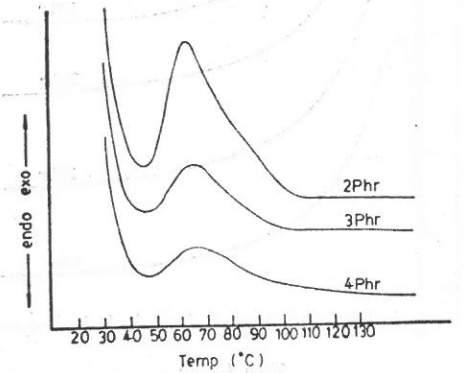

Fig. 3. Effect of initiator content on the degree of curing.

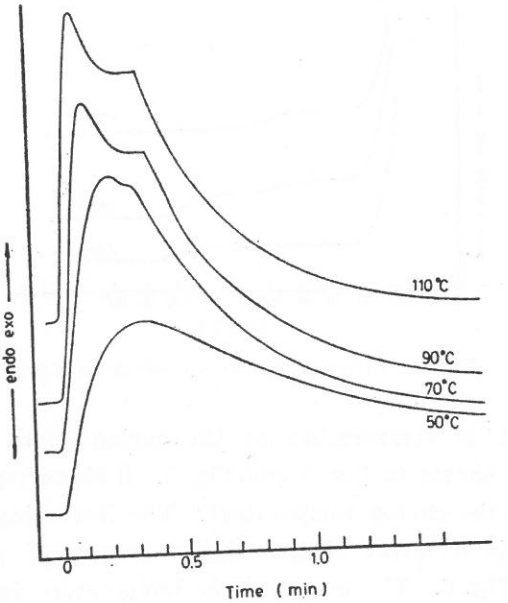

Fig. 4. Effect of temperature on the curing rate.

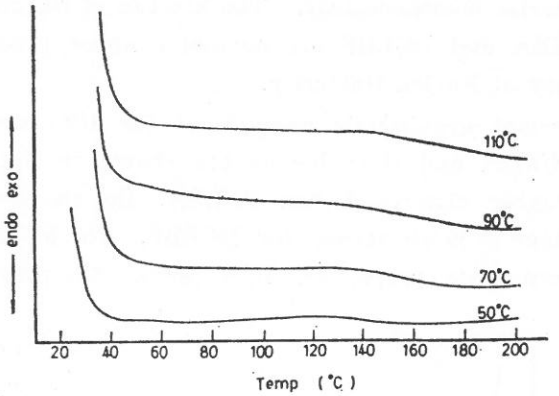

Fig. 5. Effect of temperature on Tg's.

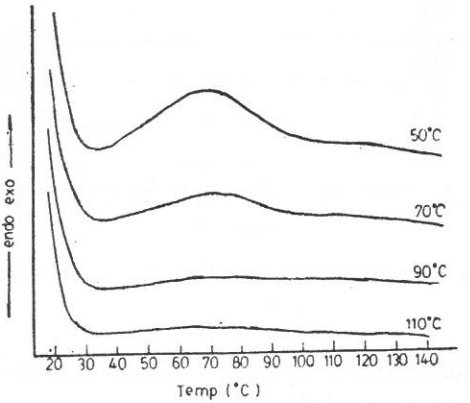

Fig. 6. Effect of temperature on the degree of curing.

When comparing the thermal stability of DGEBA with its counterpart, DGEBF, the latter exhibits a profound increase in the thermal stability, as shown by high Tg's, oxygen index values and char yield values. However, photocrosslinking of DGEBF resins was not reported before. The Tg's of UV cured DGEBF resin, DGEBA resin, and their blends are shown in Fig. 7. The glass transition temperatures of neat DGEBA and EGEBF are 140°C and 22°C respectively. Upon blending, the mixed system of DGEBA and DGEBF shows several Tg's. This indicates that the mixture does

not copolymerize homogeneously. The kinetics of the copolymerization of DGEBA and DGEBF are currently under investigation in the laboratory at Fu Jen Univerity.

The thermal gravimetric analysis of the UV cured films of DGEBA, DGEBF, and their blends are shown in Fig. 8. DGEBF exhibits a higher char yield than DGEBA. But the weight loss in the early stage is more serious for DGEBF. The blended mixture exhibit intermediate properties. By changing the ratio of DGEBA

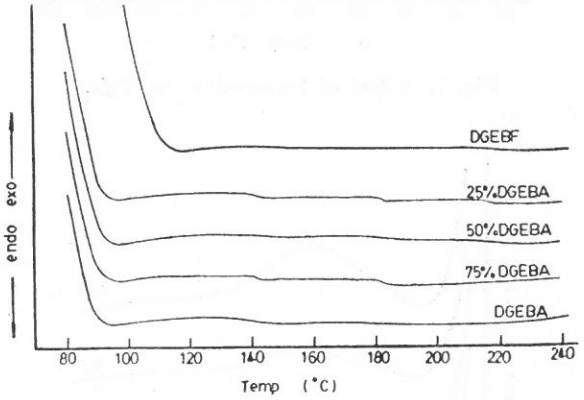

Fig. 7. DSC analysis of UV cured hybrid resins.

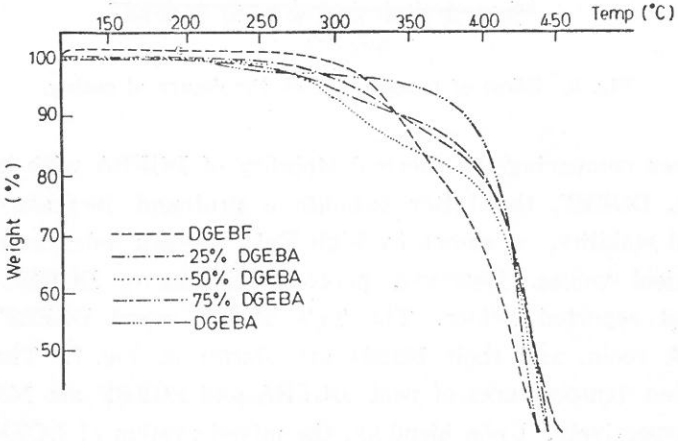

Fig. 8. TGA analysis of UV cured hybrid resins.

and DGEBF, it is possible to tailor the end-property of the cured film.

3. CONCLUSION

There is increasing interest in photopolymer systems of epoxy resins which give very good properties when crosslinked. This work demonstrates that curing temperature and initiator content have profound influence on the photopolymerization of epoxy resins. We also demonstrate that DGEBF resins are UV curable with diphenyliodonium hexafluorophosphate as photoinitiator. The resulted films exhibit higher Tg's and char yield values. By compounding DGEBA with DGEBF, epoxy resins with different thermal properties can be made.

4. EXPERIMENTAL

a. Preparation of Diphenyliodonium Hexafluorophosphate

Into a 500 ml, three necked, round bottomed flask equipped with a paddle stirrer, addition funnel, thermometer, and condenser were placed 100 g potassium iodate, 100 ml acetic anhydride, and 90 ml benzene. This mixture was cooled to −5°C and then a solution composed of 70 ml concentrated sulfuric acid and 100 ml acetic anhydride was added dropwise via the addition funnel. During the addition, the temperature was not permitted to rise above 5°C. When the addition had been completed, the reaction mixture was allowed to rise to room temperature. After standing for 48 hours, the reaction mixture was again cooled to 5°C and then 200 ml distilled water was added at such a rate that the reaction temperature did not exceed 10°C. At this point, 75 ml diethyl ether was added and the reaction mixture was filtered to remove $KHSO_4$. The aqueous solution was then added with 200 ml KPF_6 solution, containing 80 g KPF_6. After stirring, the diphenyliodonium hexafluorophosphate was filtered off, washed and dried in vacuum at 60°C to give 60% yield of product; mp 192-195°C.

b. Preparation of Deglycidyl Ether of Bisphenol Fluorene[9]

A reaction kettle equipped with a thermometer, a mechanical stirrer, and a water-cooled condenser, was charged with one mole of 9,9′-bis (4-hydroxphenyl) fluorene and 8 moles of epichlorohydrin. The stirrer was started and the reaction mixture was heated to 90°C. Over a period of 3 to 4 hours, 2 moles of sodium hydroxide pellets were added to the reaction mixture and the reaction temperature was maintained between 90 and 100°C. The reaction mixture was filtered to separate the solid sodium chloride formed during the reaction. The salt cake was then washed with additional epichlorohydrin and the unreacted epichlorohydrin was distilled off under a vacuum of 30 mm Hg from the filtrate. After no additional epichlorohydrin could be removed, the vacuum was further decreased to 2mm Hg for 30 min. at 170°C. A white crystalline powder was obtained by recrystalization of the residue from acetone/absolute ethanol.

c. DSC Calorimetric Analysis of the UV Curing System

A modified differential scanning calorimeter employed for the curing rate study was equipped according to Moore's report.[11] The UV light source is a Hanovia 450W medium pressure mercury lamp. The DSC machine is manufactured by E. I. DuPont Co.

d. UV Curing of Epoxy Coatings

The UV curing machine is equipped with a medium pressure mercury lamp (80W/cm) and a conveyor. The machine was manufactured by C-Sun Industrial Ltd., model No. UV C-101.

e. ERL-4221 and ERL-4206 are commercial products of Union Carbide

DGEBA employed in the experiment is Epon-828 of Shell Chemical Co.

REFERENCES

(1) H. Lee and K. Neville, "*Handbook of Epoxy Resins*", McGraw-Hill, New York, 1967.

(2) J. Licary and P. Crepeau, *U.S. Patent* 3, 205, 157 (1965).
(3) J. Crivello, *Ann. Rev. Mater. Sci.*, 13, 179 (1983).
(4) J. Crivello and J. Lam, *J. Polym. Sci. Polym. Chem. Ed.*, 17, 1059 (1979).
(5) J. Crivello and J. Lam, ibid, 17, 977 (1979).
(6) J. Crivello in "*Developments in Polymer Photochemistry-2*", Ed. N. Allen, 1981, p. 1, London: Applied Science Publishers.
(7) S. Pappas, "*UV Curing: Science and Technology*", 1978 Stamford, Connecticut: Technology Marketing Corp. (see especially J. Crivello, p. 24).
(8) J. Crivello and J. Lam, *J. Polym. Sci. Symp.* 56, 383 (1976).
(9) S. Lin and E. Pearce, *J. Polym. Sci. Polym. Chem. Ed.*, 17, 3095 (1979).
(10) J. Kennedy, "*Cationic Polymerization*", 1982 New York, John Wiley & Sons, Inc.
(11) J. Moore, S. Schroeter and A. Shultz, *ACS Coating and Plastics Preprints*, 35, vol 1, 239 (1975).

"Always remember your first obligation is to your *conscience.*"

Often during my boyhood I heard these words repeated by my grandfather, who was a clergyman. It was his private sermon to me; his personal version of Shakespeare's "To thine own self be true."

His words still make good sense. Who among us is not from time to time driven to make a decision between *conflicting demands?* A public servant or private citizen, all of us are often tempted to compromise on the easy, pleasant course. By doing one thing, we sidestep embarrassment. By doing another we gain immediate applause. By doing a third we quiet the loudest voices. How, then, can we determine the right thing to do?

My grandfather's answer was always the same: "*Remember your first obligation is to your conscience.* If you have to make a difficult decision, ask yourself how your conscience will react to it tomorrow, the next day and the next year. If you have any qualms, then that decision is wrong. Change it."

SENATOR IRVING M. IVES

SCANNING ELECTRON MICROSCOPE STUDIES ON POLLEN GRAINS AMONG THE FORMS OF KIRISHIMA AZALEA

CHING-SHIA CHEN

ABSTRACT

Rhododendron obstusum Planch var. *sakamotoi* Komatsv (Kirishima Azalea) is a variety of the Ericaceae. It has many forms in Taiwan. The flowers are of many colors. The types of corolla are funnel shaped and have double petals. In general we use the morphological characteristics to identify the forms; but classification of forms is also possible if we examine pollen grains with the Scanning Electron Microscope.

INTRODUCTION

The Azalea are commonly cultivated plants in Taiwan. *Rhododendron obtusum* Planch var. *sakamotoi* Komatsv (Kirishima Azalea) is a special plant. This plant is very small and has branches. It has many flowers. The corolla has many colors and the types of the corolla are from funnel shaped to double petals. In Taiwan, there are many forms of Kirishima Azalea, and more and more cultivated hybrids are coming up. In the study of the pollen grains, we can identify the characteristics of species and varieties using the Scanning Electron Microscope (Chen 1980). It is the aim of this study to show that we can also use the SEM to identify the forms.

In the usual methods of Plant Taxonomy, we look at the morphology of Rhododendron. From Burm 1768, Blume 1823, Hook 1829, Sweet 1832, G. Don 1834, Bubge 1833, Paxton 1841, Dippol 1889, Hemsl 1895, Engler & Prantl 1897, Matsum & Hayata 1906, Kanehira 1917, Mark & Huchinson 1917, Wilson 1921, Mori 1936, Copland 1943, Liu 1926, Li 1963, Yang 1971, Li 1978, until now, we relied on their methods of taxonomy.

The study of pollen grain of Rhododendron began with

Wodehuse 1930, Yang 1952, Erdtman 1952, Faegri & Iverson 1964, Huang 1968, Erdtman & Sorsa 1971, Wang 1972. All of them used a light microscope.

The usage of the Electron Microscope started with Skavala & Pyle 1968. Since then, using the SEM to study the pollen grains became very popular by Skvarla & Pyle 1968, Ridgeway 1969, Erdtman 1969, Heslop Harrison 1969, Lynch 1975, Huber & Chen 1975, Feuer 1980, Argue 1980, Chen 1980. There is no doubt that the SEM can be used for the identification of the species and varieties of the characteristics of pollen grains (Huber & Chen 1975, Chen 1980). But the identification of the characteristics of forms was not possible until the electron microscope was invented. Especially for identifying the forms of relationships of Rhododendron pollen grains, another type of analysis was necessary.

For this purpose, the pollen tetrads of seven forms in one variety of Rhododendron were examined. There were two groups: three funnel shaped flowers and four double-petal flowers. We used the Scanning Electron Microscope for examination.

At the same time, the petals of flowers of different forms were also identified with the Scanning Electron Microscope (SEM).

The study of the morphology of a plant together with the study of the morphology of the pollen grains and the petals offer a clear way to understand the plant.

MATERIALS AND METHODS

The materials used in this study were taken directly from the fields (Grass Mountain), and photographs were made for the record. The pollen grains were obtained from field collections. Voucher numbers and collecting data are recorded in Table 1.

Pollen grains for scanning with the SEM were mounted with adhesives on specimen holders and coated with carbon and gold. The Scanning Electron Micrographs were made at Fu Jen University by Prof. Chu-Fang Lo with a JSM 15 Scanning Electron Microscope.

The photographs were taken immediately after the location of

Table 1. The collection data for *Rhododendron obtusum* Planch var. *sakamotoi* Komatsv (Kirishima Azalea) used in this study and their pollen grains as examined by C. S. Chen 1981–1982. All types of specimens are at the Biology Department Herbarium, Fu Jen University

Forms of Kirishima Azalea	Locality	Collector
1. Red funnel shaped flower	Wai-shuang-hsi Grass mountain	C. S. Chen 2997 C. S. Chen 3388
2. Orange-red funnel shaped flower	Grass mountain	C. S. Chen 3389
3. Rose-red funnel shaped flower	Grass mountain	C. S. Chen 3390
4. Purple double-petal flower	Grass mountain	C. S. Chen 3391
5. Pink double-petal flower	Grass mountain	C. S. Chen 3392
6. White double-petal flower	Grass mountain	C. S. Chen 3393
7. White and pink mixed double-petal flower	Grass mountain	C. S. Chen 3394

the desired area and the determination of the most useful magnification, 2000×.

The corolla was prepared for the same specimens. The petal pieces were excised from the air-dried corona, mounted with adhesives on specimen holders (Chapman 1976, Shaw & Smeins 1979), and coated with carbon and gold, and examined in a JSM 15 Scanning Electron Microscope at Fu Jen University. The photographs are all of the same magnification 1000×.

OBSERVATION

Rhododendron obtusum Planch var. *sakamotoi* Komatsv in Bot. Mag. Tokyo 32:14, 1918; Mori in Masmune Short Fl. From 160, 1937; Yamamoto in Journ. Soc. Trop. Agr. 5:406, 1933; Makino in Jap. Flo. I:261, 1955; Uehara in III Dec. Trees 3:442, 1959. (Fig. 1, 2, 3, 4, 5, 6, 7)

The shrub is 1–3 m high and many-branched. The young branches are clothed with brown hair. Leaves are chartaceous and dimorphic. The forms are oblong, elliptic-ovated about 1.2–1.5 cm long, and 1–1.2 cm wide. The apex and the base are acute.

The surface of both sides is densely covered with long hair. There are 2–3 flowers in the terminal. The corolla has many colors from red to white. The corolla is funnel shaped and has double petals, about 2.4–3.7 cm in diameter. The calyx is 5-lobed. The lobes are oblong-ovated, and have strigose. They have 5 stamens. The filaments are granulate spots at the base. The style and ovary are covered with long hair. Capsules are 0.6–0.7 cm long and spread with hair.

Endemic. It is cultivated in Japan since many years.

1. Red funnel shaped flower form (Fig. 1)

Pollen grains are tetrads. The tetrad is intersemiangularly spherical. The longest diameter is 47–55 μ. The globals have 3 colpates. The colpus is opened. The nexine of the colpus is granulated (Fig. 8). The sexines are granulated. The face combined with three polar views is depressed, and became circularly constricted. The baculus is well processed and round. The viscin strand combines the surface. (Fig. 8)

The cells of the epidermis are clearly separated. The epidermis of the corolla is short-vermiculated and very dense. (Fig. 9)

2. Orange-red funnel shaped flower form (Fig. 2)

Pollen grains are tetrads. The tetrad is intersemiangularly spherical. The longest diameter is 46–54 μ. The globals have 3 colpates. The colpus is opened. The nexine of the colpus is small granulated. The sexines are granulated. The face combined with three polar views is deeply depressed, and became a triangular pore (Fig. 10). The baculus is well processed. The viscin strand combines the surface. (Fig. 10)

The cells of the epidermis cover each other. The epidermis of the corolla is striated and short-vermiculated in different cells. (Fig. 11)

3. Rose-red funnel shaped flower form (Fig. 3)

Pollen grains are tetrads. The tetrad is intersemiangularly spherical. The longest diameter is 46–60 μ. The globals have 3

colpates. The colpus is opened. The nexine of the colpus is large and granulated. The sexines are very small and granular. The face combined with three polar views is deeply depressed, and became a pore (Fig. 12). The baculus is well processed and round. The viscin strand combines the surface. (Fig. 12)

The cells of the epidermis are irregular, and on some places constricted. The epidermis of the corolla is separately short-vermiculated. (Fig. 13)

4. Purple double-petal flower form (Fig. 4)

Pollen grains are tetrads. The tetrad is intersemiangularly spherical. The longest diameter is 44–53 μ. The globals have 3 colpates. The colpus is opened. The nexine of the colpus is small and granulated. The sexines are clearly granulated. The face combined with three polar views is deeply depressed, and became a large pore (Fig. 14). The baculus is well processed and very rounded (Fig. 14). The viscin strand combines the surface. (Fig. 14)

The cells of the epidermis are irregular and constricted. The epidermis of the corolla is short-vermiculated and fine striated in different cells. (Fig. 15)

5. Pink double-petal flower form (Fig. 5)

Pollen grains are tetrads. The tetrad is intersemiangularly spherical. The longest diameter is 46–62 μ. The globals have 3 colpates. The colpus is opened. The nexine of the colpus is doubled and granulated (Fig. 16). The sexines are small granulose. The face combined with three polar views is very deeply depressed, and became a large pore. The baculus are well processed. The viscin strand combines the surface. (Fig. 16)

The cells of the epidermis are arranged and regular. The epidermis of the corolla stretches out in three different directions and is long striated. (Fig. 17)

6. White double-petal flower form (Fig. 6)

Pollen grains are tetrads. The tetrad is intersemiangularly spherical. The longest diameter is 45–60 μ. The globals have 3

colpates. The colpus is opened. The nexine of the colpus has only one granulum (Fig. 18). The sexines are clearly granulose. The face combined with three polar views are very deeply depressed, and became a large irregular pore (Fig. 18). The baculus is well processed and rounded. The viscin strand combines the surface. (Fig. 18)

The cells of the epidermis are irregular and constricted. The epidermis of the corolla is densely short-vermiculated. (Fig. 19)

7. White and pink mixed double-petal flower form (Fig. 7)

Pollen grains are tetrads. The tetrad is intersemiangularly spherical. The longest diameter is 45–53 μ. The globals have 3 colpates. The colpus is opened. The nexine of the colpus is granulated (Fig. 20). The sexines are densely granulose. The face combined with three polar views is deeply depressed, and became a pore. The baculus is processed. The viscin strand combines the surface. (Fig. 20)

The cells of the epidermis are regularly arranged. The epidermis of the corolla is fine-long striated. (Fig. 21)

CONCLUSION

Rhododendron obtusum Planch var. *sakamoti* Komatsv (Kirishima Azalea) is a variety of the Ericaceae. There are many forms of them in Taiwan, and more and more cultivated hybrids appear. The morphology of the plants is the same. They are very small. The leaves are complete, coriaceous. The flowers are fascicled, and terminate on top. The corolla is many colored. There are redoues, orange-redoues, rose-redoues, purpleoues, pinkoues, and whiteoues etc. There are even mixed colored ones such as white and pink. The type of corolla is from funnel shaped to double petals. So there is a lot of variety of them.

With the morphology of the plant taxonomy, the forms of Kirishima Azalea are very distinct in color in each flower.

All pollen grains of Kirishima Azalea have a great similarity. They are tetrahedral tetrads and radially symmetrical. The global

has 3 colpates. Each colpus opens between two polar areas. The NPC is 343. The L-pattern analysis shows an OL-pattern. The sexine is granulated. Pollen grains have viscin strands combining each other.

Using the SEM, we obtained the characteristics of seven forms. They are red funnel shaped flowers, orange-red funnel shaped flowers, rose-red funnel shaped flowers, purple double-petal flowers, pink double-petal flowers, white double-petal flowers, white and pink mixed double-petal flowers.

According to these characteristics, we can divide them into funnel shaped flowers and double-petal flowers. The face combined with three polar views of the double-petal flowers is more depressed than those of the funnel shaped flowers. (Fig. 8, 10, 12, 14, 16, 18, 20)

In the funnel shaped flowers, the degrees of the face depressed are different. The red flowers are light (Fig. 8), the orange-red and rose-red flowers are deep (Fig. 10, 12). The pore of the face depressed in the rose-red flower is round, and in the orange-red flower triangular.

In the double-petal flowers, there are two kinds of faces of polar views. The white flower has an irregular pore (Fig. 18). The others have three pores (Fig. 14, 16, 20).

The face of three polar views are deeply depressed in pink flowers and in white and pink mixed flowers. They are different from the purple flowers (Fig. 14). The pink flowers and the white and pink mixed flowers are distinguished in the baculus. The pink flowers are rounder than the white and pink mixed flowers (Fig. 16, 20).

Therefore, we can differentiate the forms in pollen grains using the SEM photographs.

In the epidermis of the corolla, the best way of identification is the arrangement of the cells of the epidermis. The cells of epidermis are regular cells in the pink double-petal flowers. The cell walls are clear, and on the surface of the epidermis there are processed long-striated lines from different directions (Fig. 17).

The cells of epidermis are separated from each other in red funnel shaped flowers. The epidermis of the corolla is short-vermiculated (Fig. 9). The irregular cells are orange-red funnel shaped and white and pink mixed double-petal flowers. The epidermis of white and pink mixed double-petal flower form is fine-long-striated, and the orange-red funnel shaped flower form is striated and short-vermiculated in different cells. (Fig. 11)

The cells are constricted in rose-red funnel shaped flowers, purple double petals flowers, and white double-petal flowers. The epidermis of the corolla in the white double-petal flower is densely short-vermiculated (Fig. 19). The rose-red funnel shaped flower is separately short-vermiculated (Fig. 13). The purple double-petal flower is short-vermiculated and finely striated in different cells. (Fig. 15)

Therefore, the epidermis of corolla has a distinct characteristic in forms.

DISCUSSION

By identifying the forms of *Kirishima Azalea* with the Scanning Electron Microscope, we were able to find the characteristics of pollen grains and the epidermis of corolla. But still with the method of flower color, plant-morphology seems easier and seems to lead to better results.

In the above experiments, the epidermis of corolla were constricted by air drying method. The problem is that the types of plant cells might have been changed because of deformation during the drying process. Further investigations will be done.

REFERENCES

(1) Bowers, C. G. 1930-31, The development of pollen and viscin strands in Rhododendron catawbiense, *Bull Torrey Bot. Club* **57**, 285-314.
(2) Botanists of Taiwan 1978; *Flora of Taiwan* **IV**, 21-38.
(3) Huber, F. & C. S. Chen 1975, A study on the pollen grains of Hibiscus with the Scanning Electron Microscope, *Fu Jen Studies* **9**, 89-102.
(4) Copeland, H. P. 1943. An anatomical and taxonomical study of the Genera of Rhododendron, *Amer. Mid. Natur.* 30(3), 533-625.

Fig. 1. *Rhododendron obstusum* Planch var. *sakamotoi* Komatsv. Red funnel shaped flower form.

Fig. 2. *Rhododendron obtusum* Planch var. *sakamotoi* Komatsv. Orange-red funnel shaped flower form.

Fig. 3. *Rhododendron obtusum* Planch var. *sakamotoi* Komatsv. Rose-red funnel shaped flower form.

Fig. 4. *Rhododendron obtusum* Planch var. *sakamotoi* Komatsv. Purple double-petal flower form.

Fig. 5. *Rhododendron obtusum* Planch var. *sakamotoi* Komatsv. Pink double-petal flower form.

Fig. 6. *Rhododendron obtusum* Planch var. *sakamotoi* Komatsv. White double-petal flower form.

Fig. 7. *Rhododendron obtusum* Planch var. *sakamotoi* Komatsv. White and pink mixed double-petal flower form.

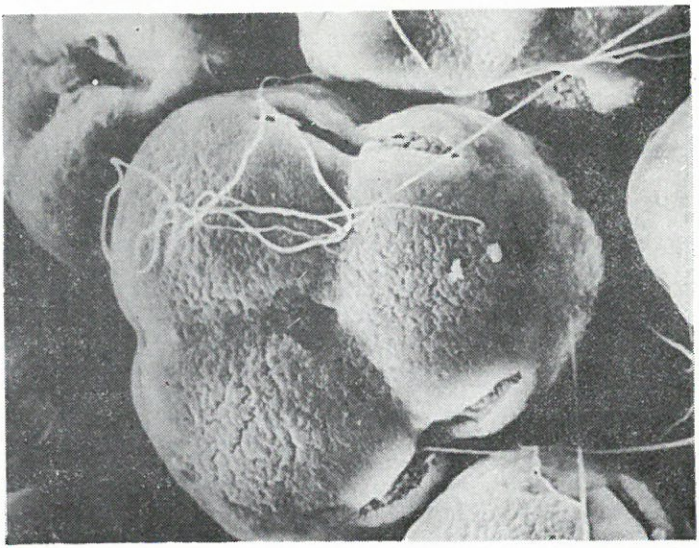

Fig. 8. Pollen grain of *R. obtusum* Pl. var. *sakamotoi* K. Red F.S. flower form. The tetrad is intersemiangularly spherical. The colpus is opened. The nexine of the colpus is granulate. The sexines are granulated. The face combined with three polar views is depressed, and became circularly constricted. The baculus is very processed and rounded. The viscin strands combine the surface. ×2000.

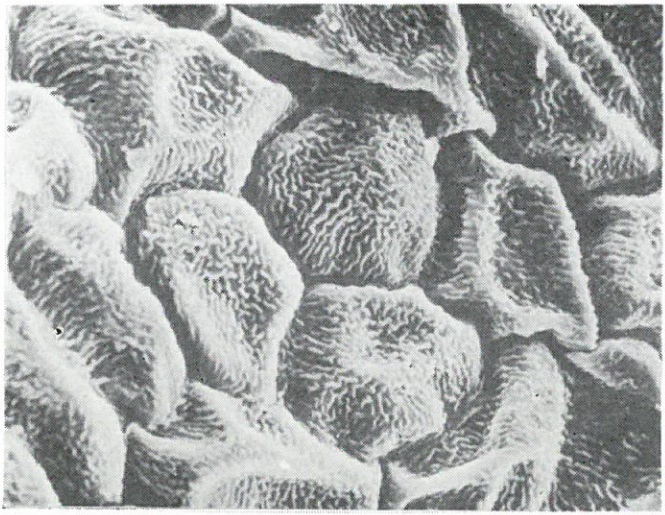

Fig. 9. The corolla of *R. obtusum* Pl. var. *sakamotoi* K. Red F. S. flower form. The cells of the epidermis are clearly separated. The epidermis of the corolla is short vermiculated and very dense. ×1000.

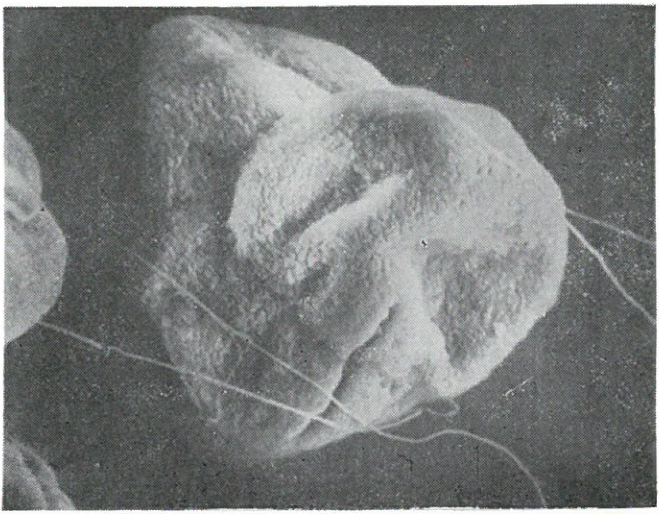

Fig. 10. Pollen grain of *R. obtusum* Pl. var. *sakamotoi* K. Orange-red F. S. flower form. The tetrad is intersemiangularly spherical. The colpus is somewhat granulated. The sexines are granulated. The face combined with three polar views is deeply depressed, and became a triangular pore. The baculus is well processed. The viscin strand combines the surface. ×2000.

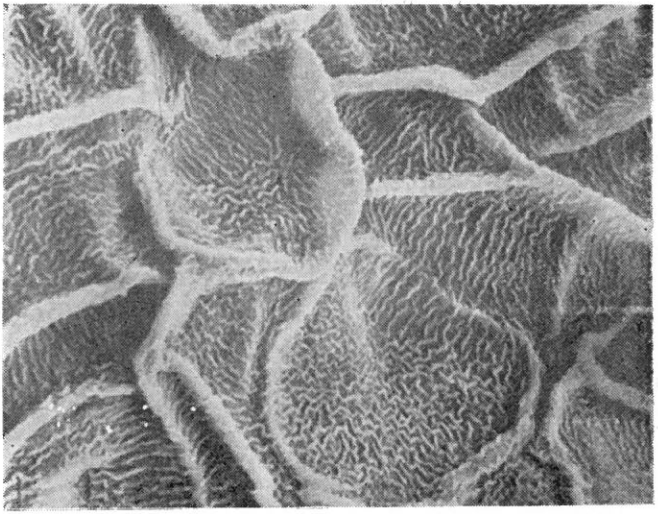

Fig. 11. The corolla of *R. obtusum* Pl. var. *sakamotoi* K. Orange-red F. S. flower form. The cells of the epidermis cover each other. The epidermis of the corolla is striated and short vermiculated in different cells. ×1000.

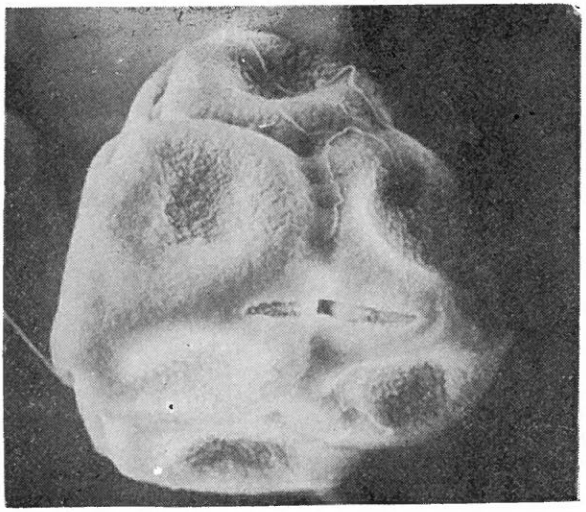

Fig. 12. Pollen grain of *R. obtusum* Pl. var. *sakamotoi* K. Rose-red F. S. flower form. The tetrad is intersemiangularly spherical. The colpus is opened. The nexine of the colpus is large and granulated. The sexines are very small and granulated. The face combined with three polar views are deeply depressed, and became a pore. The baculus combines the surface. ×2000.

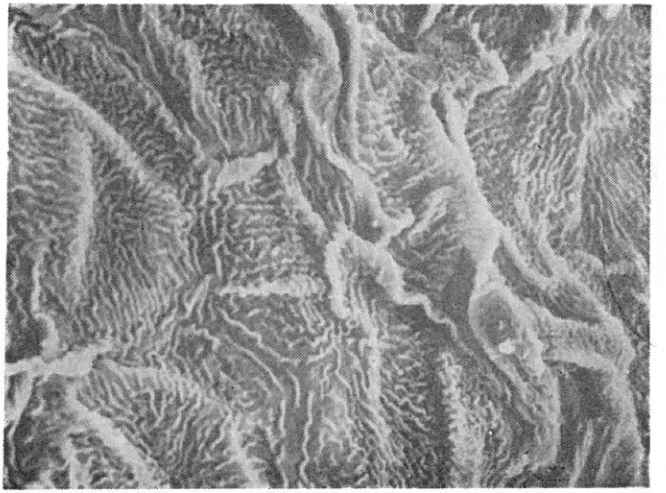

Fig. 13. The corolla of *R. obtusum* Pl. var. *sakamotoi* K. Rose-red F. S. flower form. The cells of the epidermis are irregular, and on some places constricted. The epidermis of the corolla is separately short vermiculated. ×1000.

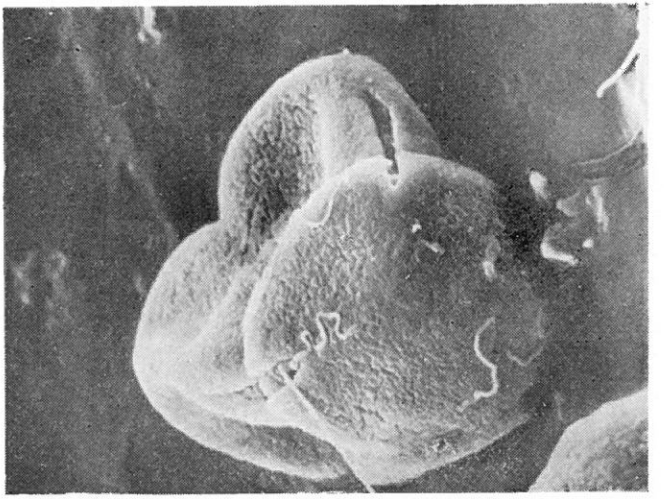

Fig. 14. Pollen grain of *R. obtusum* Pl. var. *sakamotoi* K. Purple D. P. flower form. The tetrad is intersemiangularly spherical. The colpus is opened. The nexine of the colpus is somewhat granulated. The sexines are clearly granulated. The face combined with three polar views is deeply depressed, and became a large pore. The baculus is well processed and very round. The viscin strands combine the surface. ×2000.

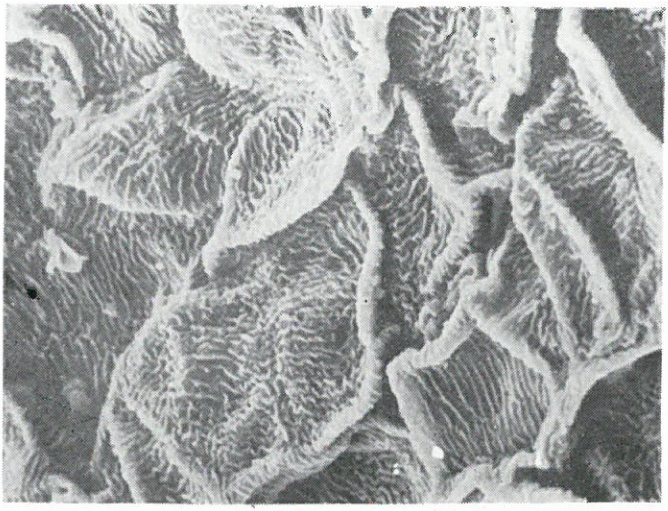

Fig. 15. The corolla of *R. obtusum* Pl. var. *sakamotoi* K. Purple D. P. flower form. The cells of the epidermis are irregular and constricted. The epidermis of the corolla is short-vermiculated and fine-striated in different cells. ×1000.

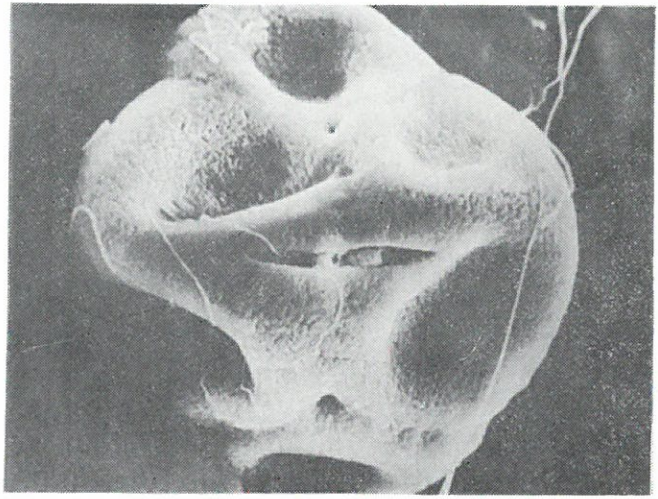

Fig. 16. Pollen grain of *R. obtusum* Pl. var. *sakamotoi* K. Pink D. P. flower form. The tetrad is intersemiangularly spherical. The colpus is opened. The nexine of the colpus has two granula. The sexines are somewhat granulose. The face combined with three polar views is very deeply depressed, and became a large pore. The baculus is very processed. The viscin strands combine the surface. ×2000.

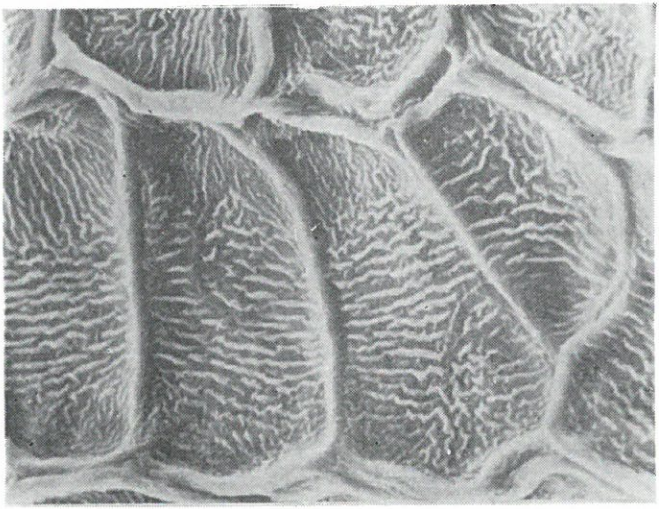

Fig. 17. The corolla of *R. obtusum* Pl. var. *sakamotoi* K. Pink D. P. flower form. The cells of the epidermis are regularly arranged. The epidermis of the corolla stretches out in three different directions and is long-striated. ×1000.

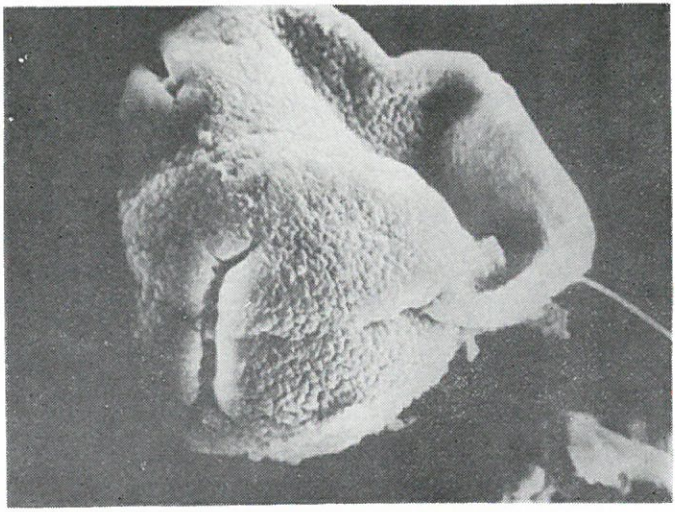

Fig. 18. Pollen grain of *R. obtusum* Pl. var. *sakamotoi* K. White D. P. flower form. The tetrad is intersemiangularly spherical. The colpus is opened, The nexine of the colpus has one granulum. The sexines are clearly granulose. The face combined with three polar views are deeply depressed, and became a large irregular pore. The baculus are well processed and rounded. The viscin strand combines the surface. ×2000.

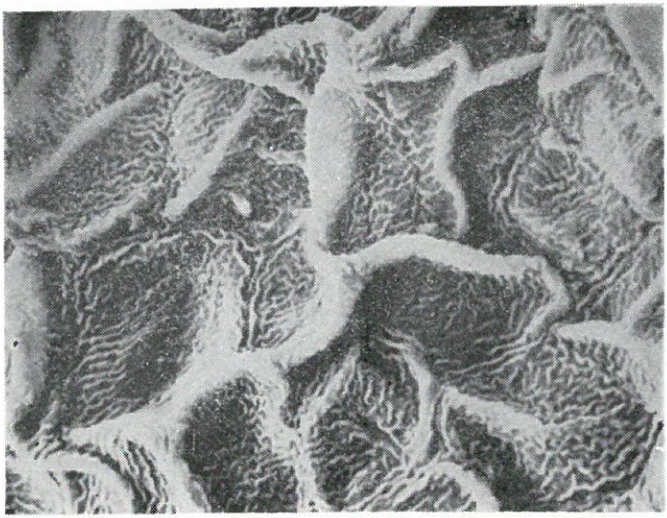

Fig. 19. The corolla of ***R. obtusum*** Pl. var. ***sakamotoi*** K. White D. P. flower form. The cells of the epidermis are irregular and constricted. The epidermis of the corrolla is densely short-vermiculated. ×1000.

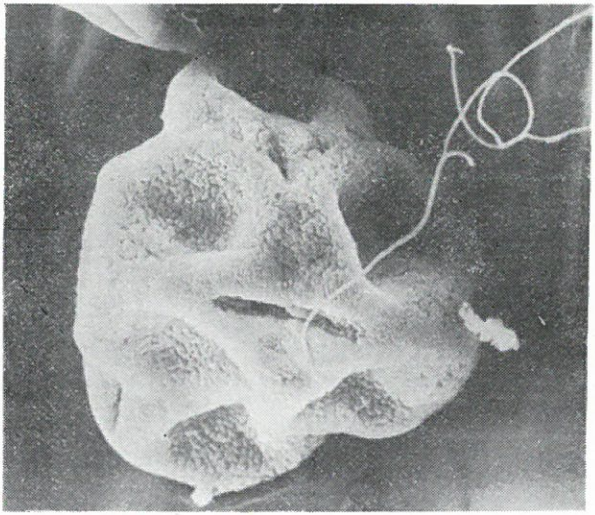

Fig. 20. Pollen grain of ***R. obtusum*** Pl. var. ***sakamotoi*** K. White and pink mixed D. P. flower form. The tetrad is intersemiangularly spherical. The colpus is opened. The nexine of the colpus is granulated. The sexines are densely granulose. The face combined with three polar views are deeply depressed, and became a pore. The baculus is processed. The viscin strand combines the surface. ×2000.

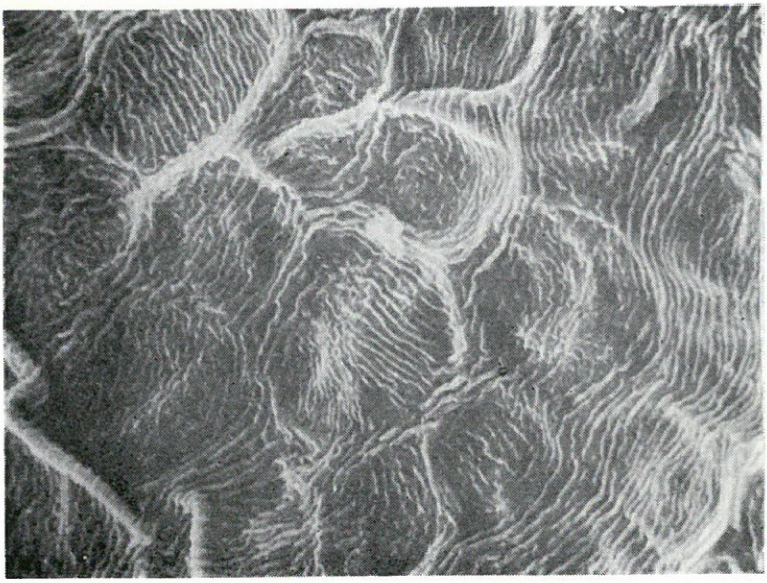

Fig. 21. The corolla of *R. obtusum* Pl. var. *sakamotoi* K. White and pink mixed D. P. flower form. The cells of the epidermis are regularly arranged. The epidermis of the corolla is fine-long-striated. ×1000.

(5) Engler, A. & Prantl 1897, *Natürliche Pflanzenfamilien*, Teil. IV 15, 65.

(6) Erdtman, G. 1952, *Pollen Morphology and Plant Taxonomy Part I*, Angiosperms, Chronica Botanica Waltham Mass.

(7) Erdtman, G. 1960, The acetolysis method. A revised description, *Sven. Bot. Tidskr.* **54**, 561-564.

(8) Erdtman, G. 1969, Handbook of Palynology—*An introduction to the study of pollen grains and spores*, Hafner publishing Co. New York.

(9) Erdtman, G. & P. Sorsa 1971, *Pollen and Spore Morphology and Plant Taxonomy*, Pteridophyta (text and additional Illustrations) Almqvist & Wiksell, Stockholm.

(10) Faegri, K. & J. Iverson 1964, *Textbook of Pollen Analysis*, Hafner. N. Y.

(11) Huang, T. C. 1968, Pollen grains of Formosan Plants IV, *Taiwania* 4(2), 148-150.

(12) Hutchinson, J. 1926, *Families of flowering Plant I*, Dicotyledons.

(13) Li, H. L. 1963, *Woody Flora of Taiwan*, 685-699.

(14) Liu, T. S. 1962, *Illustrations of Native and Introduced Ligneous Plants of Taiwan II*, 979-993.

(15) Lynch, S. P. & G. L. Webster 1975, A new technique of preparing pollen grain for Scanning Electron Microscopy, *Grana* **15**, 127-136.

(16) Ridgeway, J. J. Skvarla 1969, Scanning Electron Microscopy an Aid to Pollen Taxonomy, *Ann. M. Bot. Gard.* **56**, 121-124.

(17) Skvarla, J. J. & C. Pyle 1968, Techniques of Pollen and Spore Electron Microscope, Part II Ultramicrotomy and associated techniques *Grana Palynol.* 8, 255-270.
(18) Wilson E. H. & A. Rehder 1921, A Monograph of Azaleas, *Arnold Arboretum Pub. I,* 9.
(19) Yang, B. Y. 1952, Pollen Grains Morphology in the Ericaceae, *Quart. Journ. Taiwan Mus.* 5 (1), 1-24.
(20) Chen C. S. 1980, *A study on the cultivated Rhododendron of Taiwan,* Bio. Dept. Fu Jen Univ.

DIETARY FIBER IN BAKED PRODUCTS AND STARCH-SNACK FOOD SYSTEMS: REVIEW

WENLI JWUANG, S. Sp. S.

INTRODUCTION

It is believed that an optimum amount of dietary fiber can prevent gastrointestinal diseases such as constipation (Burkitt *et al.*, 1972), diverticulitis (Painter and Burkitt, 1971), bowel polyps, colonic cancer (Burkitt, 1974), and appendicitis (Burkitt, 1971, Walker *et al.*, 1973). Ischaemic heart disease (Trowell, 1972), obesity (Walker, 1964), and gallstones (Burkitt *et al.*, 1974) are also possibly related to a dietary fiber deficiency.

Current studies on the role of dietary fiber reveal that both the source and the amount of dietary fiber have changed during the last century (Friend, 1967). A marked reduction in consumption of cereals has occurred in Western diets during the past century. Along with this reduction, an increased amount of animal products, highly refined cereals, and sweet foods have been consumed (Burkitt, 1973).

To introduce fiber back into our diet, consumption of such foods as vegetables, cereals, cereal brans, bean hulls, nut skins, plant seeds, seaweeds, plant exudates, commercial cellulose, and synthetic gums will have to increase.

It is also possible to increase the level of dietary fiber in foods commonly consumed. However, increasing the level of dietary fiber in a food system may have a significant effect on the quality characteristics of a product. Food researchers have increased the amount of dietary fiber in various food products with dietary fibers. Several research papers indicated that various bakery products are feasible fiber carriers, i.e., bread (Tsen, 1975; Lorenz, 1976; Pomeranz *et al.*, 1976; Khan *et al.*, 1976; Prentice and D'Appolonia, 1977; Casey and Lorenz, 1977; and Volpe and Lehmann, 1977), cake (Rajchal *et al.*, 1975; Brockmole and Zabik, 1976; Zabik, *et al.*, 1977;

Table 1. Means and Standard Deviations of the Mean for Enzymatic Neutral Detergent Fiber Content in Commercial Whole Grain Breads, Cereals, Breads, Cookies, and Snacks[1]

Food items	% ENDF	g ENDF per 1 oz serving
Whole grain bread		
Schwarzbrot	13.50±0.02	3.85
Pumpernickel	11.33±0.36	3.25
Stollen	7.84±0.11	2.23
Awrey Heart Health Wheat Bread	7.66±0.20	2.18
Italian Rye Bread	5.21±0.04	1.48
Cereals		
Kellogg's All Bran	34.06±0.44	9.71
Kellogg's Bran Buds	33.84±0.04	9.64
Kellogg's Raisin Bran Flakes	14.72±0.15	4.20
Ralston's Wheat Chex	13.85±0.13	3.95
Kellogg's Frosted Mini-Wheats	13.55±0.19	3.86
General Mill's Wheaties	10.57±0.55	3.01
Food Club Raisin Bran Flakes	8.80±0.11	2.51
Grape-Nut Cereal	7.54±0.45	2.15
Kellogg's Country Morning	6.34±0.30	1.81
Nature Valley's Nature Cereals	5.87±0.43	1.67
General Mill's Total	5.81±0.19	1.66
Nature Valley, Granola Cinnamon & Raisin Cereal	5.63±0.25	1.60
C. W. Post Family Style Cereal	4.56±0.28	1.30
Cap'n Crunch Crunch Berries	3.84±0.18	1.09
Cookies and snacks		
Doritos Tortilla Chips	32.44±0.46	9.25
Sesame and Bran Sticks	16.10±0.12	4.59
Corn Chips	14.11±0.04	4.02
Potato Chips	12.64±0.28	3.60
Sesame Buds	10.85±0.12	3.08
Nature Valley Granola Bar with Coconut	8.09±0.10	2.31
Old Fashioned Oatmeal Cookies	5.43±0.16	1.55
Fig Bar	4.25±0.16	1.21

Food items	% ENDF	g ENDF per 1 oz serving
Crackers and European Crisp Breads		
Sijan Swedish Rye Crisp Bread	36.27±0.31	10.34
Ideal Flat Bread, Norwegian	28.23±0.28	8.05
Rogga	25.40±0.36	7.24
King's Crisp Bread	25.21±0.22	7.24
Crisp Bread with Linseed	22.44±0.09	6.40
Mors Flat Bread	17.77±0.15	5.05
Crisp Bread with Sesame	16.44±0.26	4.69
Triscuit whole wheat	14.67±0.42	4.11
Wheat Square Crackers	5.41±0.41	1.54
Honey Sorghum	4.76±0.29	1.36
Hearty Wheat Snack Cracker	3.67±0.38	1.05
Other food stuffs		
Red Wheat Bran	40.81±0.12	
White Wheat Bran	39.77±0.14	
Wheat Germ	24.26±0.14	
Sesame Seeds	14.36±0.10	
Jiffy Bran Muffin Mix	9.67±0.08	
Whole Grain Natural Rice	5.97±0.18	
Rolled Oat	5.63±0.28	

(1) Jwuang (1978)

Shafer and Zabik, 1978), biscuits (Brys and Zabik, 1976), sugar-snap cookies (Khan *et al.*, 1976; Casey *et al.*, 1977; and Vratanina, 1978) and snack foods (Jwuang, 1978).

Jwuang and Zabik (1979) assessed the potential dietary fiber contribution of selected commercial foods and home-prepared quick and yeast breads; over 40 commerically available breads, European crisp breads, breakfast cereals, crackers, snack foods and 10 home-prepared breads were analyzed for their Enzymatic Neutral Detergent Fiber (ENDF) content (Table 1). The commercial bread would provide from 1.5 to 3.9 g ENDF per ounce. European crisp bread contained from 4.7 to 9.7 g ENDF per ounce. Snack foods were also good sources of dietary fiber providing from

3.1 to 9.3 g ENDF per ounce, while cookies and crackers analyzed ranged from 1 to 4 g ENDF per ounce. The components of dietary fiber according to Southgate (1976) is shown in Table 2.

Table 2. Components of Dietary Fiber[1]

Principal sources in the diet	Description	Classical nomenclature
Structural materials of the plant cellwalls	Structural polysaccharides	Pectic substances, Hemicellulose, Cellulose.
	Non-carbohydrates constituents	Lignin and mineral components
Non-structural materials either found naturally or used as food additives	Polysaccharides from variety of sources	Pectic substances, Gums, Mucilages, Algal polysaccharides, Chemically modified polysaccharides

[1] Southgate (1976)

The purpose of this review includes the current food research in product development of the high-fiber baked products and the texture characteristics of the snack foods.

USE OF DIETARY FIBER IN FOOD SYSTEMS

Dietary Fiber in Cakes

Both alpha-celluloses and cereal brans have been recommended as good sources of dietary fiber for their functional bulking properties in food and nutrition. Microcrystalline cellulose has been used as a partial substitute for wheat flours in the production of muffins, cookies (Lee *et al.*, 1968), cakes and biscuits (Brays and Zabik, 1976) and mashed potatoes (Lee *et al.*, 1968) for use in low caloric diets. Zabik *et al.*, (1977) reported on substitutions with 8 kinds of celluloses (Solka-Floc BW-200, Avicel PH-101, Prototype sample #170-2, Prototype sample #174-2, Prototype #170-2 plus CMC, Prototype sample #174-2 plus CMC, Prototype sample #174-2 (85%) coated with 15% NF grade citric pectin, and 70% Prototype sample #174-2 coated with 30% NF grade citric pectin) for 30% of the cake flour in high ratio layer cakes. The results indicated that

all cakes were of good quality with few significant differences occurring among the objective and sensory data. However, cakes containing pectin-coated cellulose had compact, gummy, soggy and dough-like textures and were slightly gray in interior color.

Rajchel *et al.*, (1975) reported that up to 16% wheat bran and 12% middlings could be successfully used in place of flour and incorporated into chocolate, banana, nut and spice cakes. Brockmole and Zabik (1976) also indicated that replacement of flour with 16% wheat bran and 12% middlings in white layer cakes was acceptable. They found that the particle size of the bran used in these cakes could affect the quality characteristics. Springsteen *et al.*, (1977) indicated that the fineness of grind was important for successful incorporation of bran into cakes and found that substitution of 30% of the cake flour with a finely ground bran produced acceptable cakes. The behavior of wheat brans and other cereal brans in white layer cakes was compared by substituting three types of wheat brans (hard red, hard white, and soft red), corn bran, soy hulls and oat bran for 30% of the cake flour (Shafer and Zabik, 1978). Successful results were obtained in the layer cake systems at the level of 30% substitution of wheat and corn bran. Though cake batters containing non-wheat brans had higher batter viscosities, the resulting cakes were less tender than the cakes made with wheat bran. In addition, cakes with oat and soy bran had less pleasant flavor and were not acceptable to taste panelists. These researchers indicated that cakes could be successful carriers of dietary fiber in food system.

Dietary Fiber in Cookies

Vratanina (1978) reported that highly acceptable cookies could be formulated by incorporating red and white wheat brans up to the 30% level in sugar snap cookies, and up to 50% in oatmeal cookies. A 30% substitution of flour with wheat bran in sugar snap cookies did not significantly affect the top grain but did reduce the spread factor. Bran darkened the color and yielded more tender, less crisp cookies. Khan *et al.*, (1976) incorporated coconut residue

in sugar cookies at 5, 10, 15 and 20% levels. An excessive amount of water was required to mix an optimum sugar cookie dough when more than 10% coconut residue was incorporated. Cookies made with 20% coconut lowered the spread factor, but the aroma, taste and texture were acceptable. The crude fiber content increased from 0.14% in the control cookies to 2.02% for the 20% substituted cookies.

Dietary Fiber in Breads

Of all cereal foods, bread is the most popular (Scade, 1951). Many varieties of bread are made from whole grain meals and whole grain brans. Bakery scientists have reported that breads can be a feasible carrier of dietary fiber. Whole wheat flour and from 5 to 16% wheat bran can be satisfactorily substituted for white flour in bread and muffins (Pyler, 1973). Defatted corn-germ flour which contains 15.9% dietary fiber has been partially substituted for flour in bread. Acceptable corn-germ bread having a specific volume of more than 6.00 cc/gm could be prepared from wheat flour replaced with 12% of corn-germ flour (Tsen, 1975). Tsen reported that by using a stronger wheat flour (13.6% protein and 0.53% ash), an acceptable bread could be produced with 18% corn-germ flour.

Coconut residue is a fiber-rich byproduct (16% crude fiber) obtained from the aqueous processing of fresh coconut. Replacement up to 10% of wheat flour with coconut residue in white pan bread yielded an acceptable product (Khan *et al.*, 1976). This coconut bread contained approximately 7.5% crude fiber.

Lorenz (1976) reported that replacing up to 15% of wheat flour with brans from triticale and rye increased farinograph absorption and decreased mixing time and mixing tolerances. Amylograph studies of blends of wheat flour and triticale bran showed that these were less viscous probably because of a high alpha-amylase activity in the bran sample. Fine bran caused greater changes in viscosity than coarse bran samples. Good quality breads were baked with the fine bran samples, up to replacement levels of 15%. There was no decrease in bread volume. Proof time of breads with 10% and

15% bran were shorter than those of control breads. Loaves baked with 10% and 15% fine bran samples were softer than the control loaves after 6 days of storage. The importance of bran particle size in determining bread baking characteristics was apparent.

Pomeranz *et al.*, (1976) used wheat bran, all malt spent grains, and malt-grits spent grains to replace wheat flour at levels of 0, 3, 6, 7, 10 and 15% to produce high fiber breads. They found that all three fibrous materials increased water absorption. The increase was largest for the malt-grits replacement and smallest for wheat bran. The loaf volume decreased and the crumb grains were impaired with increasing fiber replacement levels. The decreased bread loaf volume was due to dilution of gluten protein from the substitution of various fibrous materials. As a result, the bread made from white bran-enriched wheat was superior in loaf volume, crumb grain and crumb color to the bread in which the brewer's spent grains and all malt-corn grits were added.

Prentice and D'Appolonia (1977) made high fiber bread containing brewer's spent grain (BSG) at 5, 10, and 15% levels of substitution. Consumer panels accepted favorably the bread made with the BSG for flour at 5 and 10% levels of replacement. Crude fiber and acid-detergent fiber were approximately double in flour with 10% BSG substitution.

Volpe and Lehmann (1977) used 10% alpha-cellulose blend (88.6% alpha-cellulose and 11.4% Vital wheat gluten) to replace wheat flour in 70/30 sponge-dough method. As a result, bread which contained cellulose had a lower loaf volume than either the unbromated or bromated control breads. The over-all quality of the bread containing cellulose was lower than the control bread for most of the characteristics evaluated. The addition of fiber to the bread had a slight darkening effect on the crumb. The fiber bread required more for compression at the end of seven days, but the amount was not significantly higher than the control bread. The use of alpha-cellulose in white pan bread was found to be feasible. Over-all quality of the bread was affected by the addition of fiber, but the products were acceptable.

Millet as Dietary Fiber Source in Flat Bread and Cookies

Since the cellulose and hemicellulose levels in millet are high, millet is another source of dietary fiber. It is mostly consumed locally in Northern China, India, Africa and Southern Russia (Casey and Lorenz, 1977). Leavened breads cannot be made from 100% millet, since it does not contain gluten-forming proteins (Badi *et al.*, 1976). The use of millet flour leads to rather compact pan breads with dense texture (De Rutter, 1972). Therefore millets must be baked into flat breads, as is done in Eastern Europe and Africa. In the Western world millet flour has been substituted in bread, cookies, and biscuit formulations for part of the wheat flour. This results in a different and distinct flavor in these baked products. However millet flour alone does not produce acceptable cookies. Addition of soybean lecithin for millet flours at the 0.6% level greatly improved top grain and cookie spread. The quality of these cookies, however, was not that of cookies made solely with wheat flour. Biscuits formulated with millet flour and 10% wheat flour were given acceptable consumer responses in Nigeria (Casey and Lorenz, 1977).

Carrot as Vegetable Dietary Fiber in Chips

Carrot chips were prepared from a wheat chip formulation, substituting 0 to 40% carrot powder and/or a combination of 12 to 26% carrot powder with 4 to 8% commercial cellulose for wheat flour, to study the feasibility of producing a high vegetable fiber snack. The result indicates that incorporation of carrot powder and cellulose into the carrot chip formulation improved color, texture, and flavor quality characteristics. Substituting with carrot powder up to 40% and cellulose up to 8% produced carrot chips with 7.43 and 12.58% Enzymatic Neutral Detergent Fiber respectively (Jwuang, 1978).

STRUCTURAL FORMATION IN STARCH-BASED SNACK CHIPS

The basic dough processing technique of extruded starch-based

snacks is similar to the dough formation of any baked product. Cereal flours can be used to control both the rheology of the fabricated system and a variety of textural functions such as mouth feel and consistency of foods. Coarseness or smoothness in the fabricated structure can be modified by granulation of the cereal flour. Products formulated with cereal starches may range in texture from light, fragile, highly puffed open cell structures to a dense, crisp product with very close cell structures. These snacks are normally processed by extrusion or a similar process, and followed by baking or deep-fat frying (Feldberg, 1969).

Transformation of Dough into Chips

In general, snack chips are prepared by mixing dry ingredients and liquid to form a dough with a moisture content from 25 to 45%. The dough is kneaded until it becomes pliable and forms a thin sheet. Pieces are cut from the thin dough sheet using a rotary or dicer of the extruder and are deep-fat fried to a final moisture content of 0.2 to 5.0% (Campbell and Liedman, 1976).

As materials are substituted for wheat flour, water must be added proportionately to the level of the water holding capacity of the material substituted (Jwuang, 1978). The total moisture content of the dough may vary somewhat depending on the particular starchy food material being used, but it will range from 25 to 45% by weight (Robbins, 1976). The desirable moisture level is about 40%.

During the deep-fat frying process, starch components of the wheat flour upon gelatinization absorb a great amount of the available moisture from the hydrated gluten and pentosans. They thus become thermoplastic and develop a distinct structure (Smith, 1976). According to Sandstedt (1961) starch functions to dilute the gluten, to provide a surface for union of gluten, and to become flexible during gelatinization and provide a structure permeable to gas so that baked breads do not collapse on cooling. In snack chips, gelatinized starch also lends a brittle texture to the finished product.

Shortening is also an important ingredient in snack dough

formation. It functions as a lubricant and shortening agent. The selection of the type of shortening is important for textural properties.

Other ingredients, selected for functional characteristics include leavening agents such as sodium-aluminum sulfate (SAS) baking powder to give a crumb texture to the chips. SAS baking powder produces carbon dioxide to modify the quality of the chip and results in an optimum amount of friability, density, and crispness (Jwuang, 1978).

The addition of seasonings makes the product unique and acceptable to the snack consumer. The method of introducing seasoning into the spicy products is done by dusting or spraying the seasoning over the finished snack after frying or baking (Nadison, 1969). Dusting or spraying is advantageous because it allows for the application of a large variety of seasonings. Also the seasoning is not exposed to extremely high temperatures, which minimizes the escape of volatile aroma components.

The Functional and Rheological Characteristics of Dough Components

Wheat flour is the best source for the development of a dough with good extensibility and elasticity. The protein and starch components of wheat flour contribute to the main structure of the dough and to the finished products. Addition of tuber materials such as cassava and yam increases water absorption and modifies dough structure because of the dilution effect on gluten (Ciacco and D'Appolonia, 1977). The dilution of wheat flour with cassava has been found detremental to the wheat protein quality. The addition or replacement of the part of the flour with non-gluten materials such as fiber, bran, and commercial cellulose shortened the gluten strength and impaired the quality characteristics of the baked products. The extensibility of dough decreased as starch or non-gluten materials increased (Heaps and Coppock, 1968; Jwuang, 1973). In contrast to baked products, snack chips possess a dense, crisp and close cell structure. To obtain satisfactory handling

characteristics, snack chip dough should have enough cohesiveness and extensibility to stick together as a sheet, but not have so much elasticity that it resists extension. Therefore, some dilution of wheat gluten to reduce the elasticity is beneficial.

Mixing of the snack chip ingredients yields an apparently homogeneous mass (Bushuk, 1966). At the beginning of the mixing process, a mass or wet lump with little cohesiveness is formed. Gradually the cohesiveness increases, and the dough develops elastic properties and begins to pull away from the mixing bowl. Continued mixing makes the dough smoother and its appearance drier (dough development). The function of mixing is at least twofold: even distribution of the ingredients, and development of gluten structure. These changes are accompanied by hydration of the ingredients, which is facilitated by blending. Hydration of protein is a condition for gluten development. This development is based on the formation of a network of protein molecules with occasional cross-links.

The rheological properties of dough are primarily determined by its continuous phase, the swollen protein. This continuous phase contains the gluten proteins which form thin extensible and compressible films. The snack chip dough must be sufficiently rigid to form a thin sheet that can withstand rolling yet still remain a continuous mass, so that large surface blisters will not be formed during frying (Robbins, 1976).

The viscous and elastic properties of dough are primarily due to the properties of its continuous or gluten phase. The rheological properties of such a network greatly depend on the number and strength of the cross-links between the protein molecules (Heaps *et al.*, 1967).

The insolubility of the gluten proteins is due to their intermolecular hydrogen bonds (Redman and Ewart, 1967). The viscous flow is a result of the thio-disulfide interchange reaction in the protein network. Thio-disulfide interchange during mixing causes the formation of a protein network in dough, in which protein molecules originating from different flour particles are cross-linked one with another. In this way they form a continuous and coherent

phase. The observation that the interchange reaction is most rapid in wheat flour dough, slower in doughs from rye, and still slower in dough from other cereals may offer an explanation for the differences in gas retention between these doughs (Redman and Ewart, 1967).

In general, there is a correlation between the resistance to mixing and between dough development times as determined with various recording mixers. In the same way there is a correlation between the resistance to deformation and between the extensibilities of the curve provided by various load-extension meters. Dilution of gluten will result in low resistance to mixing and a short time dough development.

When a dough is formed, water is taken up by the flour constituents in proportion to their capacity. Bushuk (1966) indicated that about 46% of water in dough is associated with starch, 31% with gluten, and 23% with pentosans. Wheat flour contains approximately 2% pentosans; they form a soft gel upon hydration and contribute significantly to dough consistency. Since pentosan molecules can not penetrate the starch granule, they form an intimate association with the gluten in which the starch granules in a dough system are embedded. Bechtel *et al.*, (1971) indicated that pentosans from wheat flour could readily disperse in water, forming highly viscous solutions. D'Appolonia and Kim (1976) reported that water insoluble pentosans interact with gluten to increase the resistance of dough to extension thus decreasing its extensibility. It has been postulated that pentosans and glycoproteins are present as transitional compounds, which play a part in the physical association and chemical bonding between carbohydrates and proteins. Patil *et al.*, (1975) found that the hydrogen bonding capacity of water-soluble pentosan molecules intensified the association between carbohydrate and protein constituents in the dough formation. It is not known if water-insoluble pentosans play a similar role. The water-insoluble fraction of the wheat endosperm cell walls are arabinoxylans, which are held within the cell wall structure by ester linkages between adjacent arabinoxylans and other cell wall

polysaccharides.

There are some differences in the basic expanded products, principally in texture and eating qualities (Nadison, 1969). The type of extruder and process used to produce the basic product can alter snack chip characteristics. Basic formulations may vary somewhat, depending upon whether the product is produced by hot or cold extrusion, and whether the resulting extruded product is baked or fried.

REFERENCES

Badi, S. M., Hoseneg, R. C. and Finneg, P. L. 1976. Peal millet. II. Partial characterization of starch and use of millet flour in breadmaking. *Cereal Chem.* 53, 718.

Bechtel, W. G., Geddes, W. F., and Gills, K. A. 1971. Carbohydrates, p. 277. In: "Wheat Chemistry and Technology". *American Association of Cereal Chemists, St. Paul, Minn. Y. Pomeranz (ed).*

Brodribb, A. J. M., and Groves, C. 1978. Effect of bran particle size on stool weight. *Gut*, 19, 60.

Brockmole, C. L. and Zabik, M. E. 1976. Wheat bran and middlings in white layer cakes. *J. Fd. Science* 41, 357.

Brys, K. D. and Zabik, M. E. 1976. Microcyrstalline cellulose replacement in cakes and biscuits. *J. Am. Diet. Assoc.* 69, 50.

Bushuk, W. 1966. Distribution of water in dough and bread. *Baker's Dig.* 40(5), 38.

Burkitt, D. P. 1971. The aetiology of appendicitis. *Br. J. Surgery* 58, 695.

Burkitt, D. P. 1973. Low residue diets and haitus hernia. *Lancet* 2, 128.

Burkitt, D. P. 1974. An epidemiologic approach to cancer of the large intestine. *Dis. Colon Rectum* 17, 456.

Burkitt, D. P., Walker, A. R. P., and Painter, N. S. 1972. Effect of dietary fiber on stools and transit time and its role in the causation disease. *Lancet* 2, 1408.

Campbell, G. M. and Liedman, S. G. 1976. *U. S. Patent* 3,937,848.

Casey, P. and Lorenz, K. 1977. Millet: Functional and nutritional properties. *Baker's Dig.* 51(1), 45.

Ciacco, C. F. and D'Appolonia, B. L. 1977. Functional properties of composite flours containing tuber flour on starch. *Baker's Dig.* 51(5), 46.

D'Appolonia, B. L. and Kim, S. K. 1976. Recent development on wheat flour pentosans. *Baker's Dig.* 50(3), 45.

De Ruiter, J. 1972. Summary of an inquiry on work done in the field of composite flours. *Institute for cereals, flours, and bread. TNO. Wageningen, the Netherlands.*

Feldberg, C. 1969. Extruded starch-based snacks. *Cereal Science Today.* 14(6), 211.

Friend, B. 1967. Nutrients in United States food supply: A review of trends, 1909-1913 to 1965. *Am. J. Clin. Nutr.* 20, 907.

Heaps, P.W. and Coppock, J.B.M. 1968. Rheology of wheat flour doughs in relation to baking quality. Symposium: Rheology and texture of foodstuffs. *Soc. Chem. Ind. London, Monograph No.* 27, 168.

Heaps, P.W., Webb, T., Russell Eggitt, P.W. and Coppock, J.B.M. 1967. Studies on mechanical factors affecting dough development. *J. Food Technology* 2, 37.

Jwuang, W., 1978. Carrot chip development and other sources of dietary fiber. Master thesis, Michigan State University.

Jwuang, W. and Zabik, M.E. 1979. Enzyme Neutral Detergent Fiber Analysis of selected commercial and home-prepared foods. *J. Food Science* 44, 924.

Khan, M.N., Hagenmaier, R.D., Rooney, L.W., and Mattil, K.F. 1976. High fiber coconut products for baking system. *Baker's Dig.* 50(4), 19.

Lee, C.J., Rust, E.M., and Reber, E.F. 1968. Acceptability of foods containing a bulking agent. *J. Am. Diet Ass.*, 54, 210.

Lorenz, K. 1976. Triticale bran in fiber breads. *Baker's Dig.* 50(6), 27.

Nadison, G. 1969. Seasoning blends for expanded snack products. *Cereal Sci. Today.* 14(6), 215.

Painter, N.S. and Burkitt, D.P. 1971. Diverticular disease of the colon: A deficiency disease of Western civilization. *Br. Med. J.* 2, 450.

Patil, S.K., Tsen, C.C. and Lineback, D.R. 1975. Water-soluble pentosans of wheat flour. II. Characterization of pentosans and glycoproteins from wheat flour and dough mixed under various conditions. *Cereal Chem.* 52, 57.

Pomeranz, Y., Shogren, M.D. and Finney, K.F. 1976. White wheat bran and brewer's spent grains in high fiber.

Prentice, N. and D'Appolonia, B.L. 1977. High fiber bread containing brewer's spent grains. *Cereal Chem.* 54, 1084.

Rajchel, C.L., Zabik, M.E. and Everson, E. 1975. Wheat bran and middlings —a source of dietary fiber in banana, chocolate, nut and spice cakes. *Baker's Dig.* 49(3), 27.

Redman, D.G. and Ewart, J.A.D. 1968. Disulfide interchange in cereal proteins. *J. Sci. Fd. Agri.* 18, 520.

Robbins, P.M. 1976. Convenience food recent technology. *Noyes Data Corporation*, New Jersey.

Sandstedt, R.M. 1961. The function of starch in the baking of bread. *Baker's Dig.* 35(3), 36.

Scade, J. 1951. An anthology of bread. In: The Story of Bread. *National Bakery School, London.*

Shafer, M.A.M. and Zabik, M.E. 1978. Dietary fiber sources for baked products: Comparison of wheat brans and other cereal brans in layer cakes. *J. Fd. Sci.* 43, 375.

Smith, O.B. 1976. Why extrusion cooking. *Cereal Food's World.* 33(2), 121.

Southgate, D.A.T. 1976. *The chemistry of dietary fiber.* In: "*Fiber in Human Nutrition*". Spiller, G.A. and Amen, R.J. (EDS). Plenum Publishing Co., New York.

Springsteen, E., Zabik, M. E. and Shafer, M. A. M. 1977. Note on layer cakes containing 30 to 70% wheat bran. *Cereal Chem.* 54, 193.

Trowell, H. C. 1972. Ischaemic heart disease and dietary fiber. *Am. J. Clin. Nutr.* 25, 926.

Tsen, C. C. 1975. Defatted corn germ flour, a nutritive ingredient for bread making. *Baker's Dig.* 49(5), 42.

Volpe, T. and Lehmann, T. 1977. Production and evaluation of a high fiber bread. *Baker's Dig.* 51(2), 24.

Vratanina, D. L. 1978. Bran as a source of dietary fiber in cookies. *M. S. Thesis*, Michigan State University Library, East Lansing.

Walker, A. R. P. 1964. Overweight and hypertension in emerging populations, editorial. *Am. Heart J.* 58, 581.

Walker, A. R. P., Richardson, B. D., Walker, B. F. and Woolford, A. 1973. Appendicitis, fiber intake and bowel behavior in ethnic groups in South Africa. *Postgrad. Med. J.* 49, 243.

Zabik, M. E., Shafer, M. A. M. and Kukorowski, B. W. 1977. Dietary fiber sources for baked products: Comparison of cellulose types and coated-cellulose products in layer cakes. *J. Fd. Sci.* 42, 1428.

There are some people who are proud and wise and practical, who say that it is not in human nature *to be generous*, that men will always fight one another, that the strong will conquer the weak, and that there can be no real moral foundation for man's civilization. We can not deny the facts of their assertion that the strong have power in the human world, but I refuse to accept this as a revelation of truth....

We should know that truth, any truth that man acquires, *is for everyone*. Money and property belong to individuals, to each of you, but you must never exploit truth for your personal aggrandizement; that would be selling God's blessing for a profit. However, *science* is also truth; it has its place in the healing of the sick, and in giving more food and leisure for life. When it helps the strong crush the weak, and rob those who are asleep, it is using truth for impious ends. Those who are thus sacrilegious will suffer and be punished, for their own weapons will be turned against them.

RABINDRANATH TAGORE

CONTRIBUTORS TO THIS NUMBER

Kow-Je Ling 凌國基, professor of physics at Fu Jen University.

Ming-Chang Huang 黃敏章, graduate student in physics at Fu Jen University.

Nai-Li Huang-Liu 劉黃乃麗, professor of physics at the University of California at Riverside, USA.

Frank E. Budenholzer, SVD, 柏殿宏, professor of chemistry and director of the Graduate School of Chemistry at Fu Jen University.

Ching-Ching Lee 李卿青, research assistant in the Department of Chemistry at Fu Jen University.

Dong-Tsair Hwang 黃棟材, graduate student in chemistry at Fu Jen University.

Jonq-Min Liu 劉仲明, associate professor of chemistry at Fu Jen University.

Sung-Nung Lee 李選能, associate professor of chemistry at Fu Jen University.

Ching-Shia Chen 陳擎霞, associate professor of biology at Fu Jen University.

Wenli Jwuang, S. Sp. S. 莊文孋, associate professor of nutrition and food science at Fu Jen University.

PRINTED BY

Ching Hua Press Co., LTD., Taipei